ACM SIGGRAPH / Eurographics Symposium on Computer Animation 2024
M. Skouras and H. Wang
(Guest Editors)

COMPUTER GRAPHICS *forum*
Volume 43 (2024), Number 8

Curved Three-Director Cosserat Shells with Strong Coupling

F. Löschner, J. A. Fernández-Fernández, S. R. Jeske and J. Bender

RWTH Aachen University, Germany

Figure 1: *Two scenes with curved geometries demonstrate our incremental potential formulation of a Cosserat shell model. It is strongly coupled to other systems through frictional contact based on "High-Order IPC" [FJZ*23]. **Left:** An initially wrinkled "sheet of papyrus" first rolls up like a scroll and is then pushed open again using three rigid bodies. **Right:** A half sphere is twisted into a "dumpling-inspired" shape, by applying an angular velocity directly to a single vertex (the "north pole").*

Abstract

Continuum-based shell models are an established approach for the simulation of thin deformables in computer graphics. However, existing research in physically-based animation is mostly focused on shear-rigid Kirchhoff-Love shells. In this work we explore three-director Cosserat (micropolar) shells which introduce additional rotational degrees of freedom. This microrotation field models transverse shearing and in-plane drilling rotations. We propose an incremental potential formulation of the Cosserat shell dynamics which allows for strong coupling with frictional contact and other physical systems. We evaluate a corresponding finite element discretization for non-planar shells using second-order elements which alleviates shear-locking and permits simulation of curved geometries. Our formulation and the discretization, in particular of the rotational degrees of freedom, is designed to integrate well with typical simulation approaches in physically-based animation. While the discretization of the rotations requires some care, we demonstrate that they do not pose significant numerical challenges in Newton's method. In our experiments we also show that the codimensional shell model is consistent with the respective three-dimensional model. We qualitatively compare our formulation with Kirchhoff-Love shells and demonstrate intriguing use cases for the additional modes of control over dynamic deformations offered by the Cosserat model such as directly prescribing rotations or angular velocities and influencing the shell's curvature.

CCS Concepts

• ***Computing methodologies*** → ***Physical simulation;***

1. Introduction

Objects with shell-like geometries such as paper, fabrics, cans, metal sheets and thin-walled 3D prints are ubiquitous in our daily lives. As such, their simulation is also of high interest in the field of physically-based animation. It is well known that for such objects, codimensional simulation as a surface embedded in three-dimensional space is beneficial in terms of computational efficiency and numerical properties in comparison to full volumetric simulations. A common approach for shells in computer graphics is to individually model in-plane stresses with an inherently two-dimensional approach (e.g. the Baraff-Witkin model [BW98; Kim20]) combined with a separate bending model based on discrete curvature measures (e.g. Discrete Shells [GHDS03; BMF03]). In the recent work of Wen and Barbič [WB23] however, it was emphasized that the application of continuum models can instead au-

tomatically lead to a unified strain energy that is consistent with volumetric models for wide ranges of shell thicknesses. Usually, such approaches are also less dependent on the orientation of edges than typical geometrically motivated bending energies. At the same time, such models maintain controllability over the deformations by explicitly identifying the effect of different energy terms which allows us to non-physically scale their influence relative to each other.

Research on continuum-based shell models in the physically-based animation community focused nearly exclusively on Kirchhoff-Love (KL) shells [WB23; CSvRV18; CTT17; TWS06; GKS02] where the main assumption is that no transverse shearing occurs (i.e. a slice of material orthogonal to the midsurface always stays orthogonal during deformation). Overall, the shape of a KL shell is entirely determined only by the positional degrees of freedom of the midsurface. Meanwhile, in the mechanics and applied mathematics community, shell models that incorporate shearing and are based on rotational degrees of freedom are much more prevalent [SF89; SFR90; SB95]. One family of such models are Cosserat models which are already long established in graphics for the simulation of one-dimensional rods [Pai02; ST07; KS16; DKWB18; SKH*21]. More recently, Löschner et al. [LFJ*23] explored the application of a Cosserat (or "micropolar") material model for the simulation of three-dimensional deformables providing explicit control over bending modes which cannot easily be achieved with classic hyperelastic materials. Taking inspiration from this work, we investigate the remaining gap of Cosserat models in physically-based animation for flat and curved shells.

The three-director Cosserat shell models that we consider in this work introduce an orthogonal frame, the orientation of three directors or unit vectors, as additional degrees of freedom. These degrees of freedom represent the *microrotation field* which models transverse shearing and in-plane "drilling" rotation of the material as illustrated in Figure 2. This in-plane rotation distinguishes the model from one-director Cosserat models such as the one presented by Weischedel [Wei12]. Several aspects make such Cosserat models an intriguing option for the simulation of shells in physically-based animation. As the bending strains of the surface are directly based on the microrotations, we do not have to rely on discrete geometric curvature measures of the positional degrees of freedom that can fluctuate for meshes of bad quality. Instead, we immediately obtain a formulation of only first-order derivatives of the degrees of freedom. It also enables us to directly apply higher-order discretizations to the shell model which is otherwise not immediately straightforward for established approaches in computer graphics. Finally, we can not only effectively control the shell's curvature, but also directly apply point- or edge-wise rotation and angular velocity constraints as well as torques or angular accelerations.

In this work, we propose a novel incremental potential formulation for the dynamic simulation of three-director Cosserat shells. As opposed to typical formulations from the mechanics literature, this allows for strong coupling to other physical system commonly used in graphics such as rigid bodies or three-dimensional deformables through frictional contact. To achieve this, we adapt an approach originally presented for three-dimensional micropolar deformables [LFJ*23] and apply it to established Cosserat

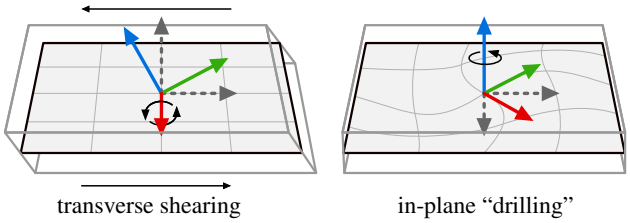

Figure 2: *Three-director Cosserat (micropolar) shells model transverse shearing and in-plane "drilling" in addition to in-plane stretching/shearing and bending modes of Kirchhoff-Love shells. The dashed and colored arrows indcate the orientation of the directors in the undeformed and deformed configuration, respectively.*

plate [SNB16] and Cosserat shell [NSBN23] models. Our contribution focusses on the analysis and validation of this approach with insights for the application in physically-based animation. We present the fundamental kinematics known in the mechanics literature from the perspective of computer graphics practitioners and highlight the required changes to the previously introduced finite element method (FEM) based solver to support codimensional curved reference configurations (Section 3.1 and 4.2). Specifically for shells, a naive discretization using first-order elements can lead to strong shear-locking even in simple scenarios. Therefore, we experimentally validate a discretization utilizing second-order elements for the shell displacements (Section 4.2). As part of our contribution, we also experimentally compare and discuss the aforementioned plate and shell models and provide insights on their parameters and the effect of individual energy terms with respect to the application in animation (Section 3.2). In this context, we motivate the use of the simpler plate model, even for curved shells, and substantiate this decision in our evaluation (Section 5). We also show that the model is consistent with the full three-dimensional model (Section 5.2). Finally, we present several compelling experiments demonstrating the additional control over the curvature of the material as well as coupling with frictional contact which can be realized due to our proposed formulation (see Figure 1).

2. Related Work

Plates and shells in graphics Even though continuum-based shell models are established in the graphics community for a long time [GTS02; GKS02], the simulation of shells with non-planar rest configurations attracted significant attention with the geometrically motivated Discrete Shells model introduced concurrently by Grinspun et al. [GHDS03] and Bridson et al. [BMF03]. Several subsequent works further analyzed and built upon this [GGWZ07; GGRZ06]. There is a large body of research which can substantially improve the results or efficiency of shell simulations such as the enhancement of coarse simulations with "wrinkle fields" [CKSV23; CCK*21] and other detail enhancement approaches [RK13; MC10; BMWG07], consistent progressive simulation with a hierarchy of meshes [ZDF*23; ZDF*22], remeshing and adaptive refinement [NPO13; NSO12; BD12; GKS02], and adaptive rigidification of shells [MK23]. While some of these methods do not necessarily build on specific shell models they would still require adaptions to apply them to Cosserat shells which is

out of scope for this publication but an interesting direction for future work. However, our incremental potential formulation directly permits coupling with other physical systems through robust frictional contact [LFS*20; LKJ21] to, e.g., rigid [FLS*21] or affine [LFJ*23] bodies or three-dimensional deformables [KE22; SB12] and other shell models.

Continuum-based shells in graphics Most continuum-based shell models in graphics are based on the Kirchhoff-Love assumption. A popular approach for their discretization is the use of subdivision surfaces [COS00] as they satisfy the strong continuity requirements of KL shells without further modifications [GKS02; TWS06; WHP11]. A different approach to deal with is by applying non-conforming discretizations such Discontinuous Galerkin methods [KGBG09; NR08]. Whereas earlier works focused on a specific material model, Clyde et al. [CTT17] generalized this to general Green strain-based materials but rely on numerical integration across a shell's thickness. In contrast, Chen et al. [CSvRV18] restrict their model to the Koiter shell energy (corresponding to the St. Venant-Kirchhoff material in the volume), allowing them to avoid the numerical integration in thickness direction and to apply a particular discretization with first-order triangles rigorously motivated by Weischedel [Wei12]. Recently, Wen and Barbič [WB23] generalized this by deriving a KL shell energy for arbitrary hyperelastic material models which does not have the typical continuity requirements of KL models through clever simplification. Beyond KL shells, Guo et al. [GHF*18] simulate shear-deformable shells by splitting the shell deformation into KL and normal/shearing modes (see also [LBC12; EOB13]) and achieve frictional contact using an MPM discretization with subdivision surfaces. While these methods all use codimensional models, Chen et al. [CXY*23] instead proposed a volumetric prism element with reduced integration, completely discarding shearing modes to avoid locking for the simulation of thick shells with arbitrary material models.

Cosserat shell models As Weischedel [Wei12, Ch. 1.3] notes, even for moderately thick shells KL models can incur large displacement errors in bending modes due to their rigidity to shearing. Together with the fact that shear-deformable models received almost no attention in physically based animation, this motivates us to investigate Cosserat models, which are shear-deformable and introduce additional rotational degrees of freedom. Cosserat models models are long established in mechanics and engineering [SF89; SFR90; SB95; DKS13] and also led to "shell elements" for thick shells with rotational degrees of freedom such as the popular MITC elements [LB04; LLB14] and others [FOZ95]. In this work, we consider three-director models which are derived from a three-dimensional Cosserat (or micropolar) continuum [NBO15]. In contrast to one-director Cosserat shells [Wei12] (see [AAE10] for a classification) they have a direct connection to previous Cosserat rod [Pai02; ST07; KS16] and micropolar deformable models [LFJ*23] in graphics. The specific models that we employ are *a)* the Cosserat *plate* model originally derived by Neff [Nef04] and numerically discretized by Sander et al. [SNB16] and *b)* the related Cosserat model for *curved shells* derived by Bîrsan et al. [BGMN19] and extended for non-orientable surfaces and numerically discretized by Nebel et al. [NSBN23]. The existing discretization approaches are mathematical elegant [San12; San15] but numerically quite involved and hard to integrate into typical frameworks used in physically-based animation. Instead, we follow a discretization approach based on the interpolation of angular velocities originally proposed for the simulation of three-dimensional micropolar deformables in animation [LFJ*23] and adapt it to shells in this work.

Higher-order elements To avoid locking we employ second-order elements for the discretization of shells (Section 4.2). The use of higher-order discretizations is generally less common in computer animation. However, there are both early works, e.g., on surface modeling with curved elements [CG91] as well as many recent works, e.g., on p-refinement [SHD*18; WMA*15], deformables [WKS*11; BC14], embedded three-dimensional deformables [LLK*20] and contact handling [FJZ*23] highlighting their benefits for different applications [SHG*22]. In the context of shells, Le et al. [LDB*23] recently proposed an adaption of the Discrete Shells [GHDS03; BMF03] bending energy for second-order triangle meshes and demonstrated the superior efficiency and accuracy of this discretization in several experiments. We share these conclusions but apply such elements to a continuum-based model. A key advantage of higher-order elements is their ability to accurately represent curved geometries. Automatically generating these meshes is an active area of research, especially in engineering [SPZ21; TPM18; FP16] with tools already available [GKT*24; YZHY19; IW18]. Alternatively, it is possible to generalize surface reconstruction methods to generate curved meshes [LZRJ19; BZKR17]. Nevertheless, the results of Le et al. [LDB*23] and our experiments (Section 5) demonstrate that second-order elements give high-quality results even for coarse meshes without such tools.

Non-Euclidean shells & controlled deformations Typical continuum-based models assume the existence of a stress-free rest state where the strain measures evaluate to zero. In contrast to this, *non-Euclidean* elasticity [SE10; ESK09] describes deformables that do not have such a stress-free configuration and exhibit internal stresses even without external forces. In simulations, such deformables can be created by prescribing a non-zero target metric of the shell for stretching and/or bending which can induce complex deformations with buckling and wrinkling [VSWH14]. Chen et al. [CSvRV18] investigated this concept in detail by proposing target metrics defined through physical models of e.g. heat or moisture distributions. For three-dimensional micropolar deformables similar effects can be achieved by prescribing a rest "wryness tensor" [LFJ*23]. Recently, Wen et al. [WWB24] proposed a method for shape modeling of surfaces which explicitly prescribes *compatible* fundamental forms such that a smooth target shape can be perfectly matched by the shell in contrast to non-Euclidean shells. Finally, example-based methods can be used for an even broader range of artistically controlled deformations [STC*12; FB11]. These methods first require a set of exemplary deformations which could be created with one of the approaches mentioned above, or with the capabilities of Cosserat shells that we demonstrate in this work.

3. Cosserat shells: kinematics & constitutive model

As Cosserat shell models are not well established in the computer graphics community, we will first present the necessary kinematic relations followed by the introduction of the constitutive models that we employ in our implementation. In comparison to the three-dimensional micropolar deformables presented in computer graphics by Löschner et al. [LFJ*23], the kinematic relations differ significantly as they now have to expressed in local coordinates on a curved surface instead of a cartesian coordinate system. With respect to the sources of the constitutive models that we implement [SNB16; NSBN23], we interpret the models and their parameters in the context of computer graphics and present insights into their effects and usage.

Notation In the following, Latin indices $i, j, k...$ range over the set $\{1,2,3\}$ and Greek indices $\alpha, \beta, ...$ range over the set $\{1,2\}$. Indices appearing twice in an equation indicate summation over the index. Vectors $\boldsymbol{e}_i \in \mathbb{R}^3$ and $\boldsymbol{e}_\alpha \in \mathbb{R}^2$ denote the three and two dimensional cartesian unit vectors. For a vector-valued function $\boldsymbol{f} : \mathbb{R}^n \to \mathbb{R}^m$, we define $[\nabla \boldsymbol{f}]_{ij} = \partial f_i / \partial x_j$, i.e. $\nabla \boldsymbol{f} \in \mathbb{R}^{m \times n}$ is the Jacobian of $\boldsymbol{f}$. We denote the axial vector of a skew-symmetric matrix $\mathbf{A} \in \mathbb{R}^{3\times3}$ with $\operatorname{axl}\mathbf{A}$ and its entries are given by $\operatorname{axl}\mathbf{A} = [A_{32}, A_{13}, A_{21}]^T$ such that $\mathbf{A}\boldsymbol{x} = \operatorname{axl}\mathbf{A} \times \boldsymbol{x}$ for all $\boldsymbol{x} \in \mathbb{R}^3$. For a matrix $\mathbf{A}$ we identify the symmetric part with $\operatorname{sym}\mathbf{A}$ and the skew-symmetric part with $\operatorname{skew}\mathbf{A}$. We denote the identity matrix with $\mathbb{1}$.

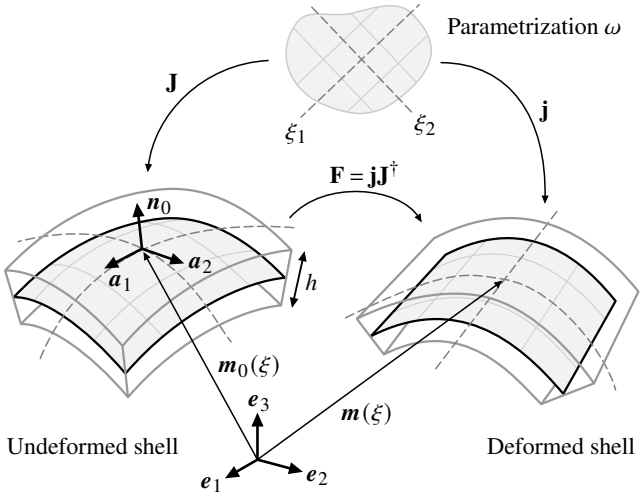

Figure 3: *The geometry of the undeformed (left) and deformed shell (right) in $\mathbb{R}^3$ is described by the midsurface embeddings $\boldsymbol{m}_0$ and $\boldsymbol{m}$, respectively, in the coordinates $\xi_\alpha \in \omega$ of the local parametrization. The maps $\mathbf{J}$ and $\mathbf{j}$ transform vectors from the parametrization space into the tangent space of the shell midsurface. Depending on the parametrization, the covariant basis vectors $\boldsymbol{a}_1$ and $\boldsymbol{a}_2$ do not have to be orthonormal.*

3.1. Kinematic relations

To model shells we only consider the midsurface $\mathcal{S}$ of a thin three-dimensional deformable with constant thickness h at rest. As we want to model arbitrary non-developable surfaces which can be closed and have holes, we cannot generally assume that a single parametrization $\omega \subset \mathbb{R}^2$ exists that covers the entire shell surface. Instead, more rigorous works introduce an abstract two-dimensional manifold that can be covered by a set of local charts that are subsets of $\mathbb{R}^2$ (realized in practice by, e.g., the parametrization of the FEM reference element). For the practical purpose of this introduction however, we disregard this distinction and assume a local parametrization $\omega \subset \mathbb{R}^2$ exists. For a more rigorous treatment which also explores the implications of non-orientable surfaces we refer to the work of Nebel et al. [NSBN23].

The physical configuration of the midsurface is described by an embedding $\boldsymbol{m} : \omega \to \mathbb{R}^3$ which maps points from the parametrization domain to their position in three-dimensional space. As for micropolar volumetric deformables, every point in the shell has an orientation which is given by the *microrotation field* $\overline{\mathbf{R}} : \omega \to SO(3)$. The microrotation field captures the out-of-plane bending of the shell and additionally characterizes its transverse shearing and "drilling" (i.e. in-plane "twisting" of the material, see Figure 2). In general, it does not have to match the macroscopic rotation of the material $\mathbf{R}$ which (for three-dimensional deformables) is uniquely determined by the polar decomposition of the deformation gradient $\mathbf{F} = \mathbf{R}\mathbf{U}$. The microrotation is an independent degree of freedom but will be coupled with the deformation by the constitutive model.

Tangent space The deformation of a shell is described using quantities in the tangent space of the surface. Following classic literature on shells, the tangent space is spanned by the covariant basis vectors $\{\boldsymbol{a}_1, \boldsymbol{a}_2\} \subset \mathbb{R}^3$. Let $\mathbf{J} = \nabla_\omega \boldsymbol{m}_0 \in \mathbb{R}^{3\times2}$ denote the Jacobian of the undeformed (rest state) midsurface embedding $\boldsymbol{m}_0$ with respect to the parametrization ω. Then, the covariant basis $\{\boldsymbol{a}_1, \boldsymbol{a}_2\}$ is given by the columns of

$$\mathbf{J} = \frac{\partial \boldsymbol{m}_0}{\partial \xi_\alpha} \otimes \boldsymbol{e}_\alpha = \boldsymbol{a}_\alpha \otimes \boldsymbol{e}_\alpha \,, \tag{1}$$

where $\xi_\alpha \in \omega$ are the coordinates of the parametrization. Note that these basis vectors are generally neither orthogonal nor normalized. The matrix $\mathbf{I} = \mathbf{J}^T\mathbf{J} \in \mathbb{R}^{2\times2}$ represents the metric tensor or first fundamental form of the surface and $\sqrt{\det \mathbf{I}}$ defines the ratio of area elements of the embedding $\boldsymbol{m}_0$ to area elements in the parametrization domain. With the surface normal at rest

$$\boldsymbol{n}_0 = \frac{\boldsymbol{a}_1 \times \boldsymbol{a}_2}{\|\boldsymbol{a}_1 \times \boldsymbol{a}_2\|} = \frac{\boldsymbol{a}_1 \times \boldsymbol{a}_2}{\sqrt{\det \mathbf{I}}} \,, \tag{2}$$

the contravariant basis $\{\boldsymbol{a}^1, \boldsymbol{a}^2\}$ is defined to fulfill the properties $\boldsymbol{a}_\alpha \cdot \boldsymbol{a}^\beta = \delta_{\alpha\beta}$ and $\boldsymbol{n}_0 \cdot \boldsymbol{a}^\alpha = 0$. In particular, the contravariant basis vectors are given by the the rows of

$$(\mathbf{J}^T\mathbf{J})^{-1}\mathbf{J}^T = \boldsymbol{e}_\alpha \otimes \boldsymbol{a}^\alpha = \mathbf{J}^\dagger \,, \tag{3}$$

where $\mathbf{J}^\dagger \in \mathbb{R}^{2\times3}$ denotes the pseudoinverse of $\mathbf{J}$. The map given by $\mathbf{J}^\dagger$ performs the expansion of any vector with respect to the covariant basis (projection into parametrization space). It follows that $\mathbf{J}\mathbf{J}^\dagger$ performs the orthogonal projection onto the tangent plane in $\mathbb{R}^3$ (i.e. it discards the normal component) and is therefore also the identity operator on this subspace [Mey00]. Let $\boldsymbol{f} : \omega \to \mathbb{R}^n$ be a vector field on the surface, then the *surface gradient* $\nabla_\mathcal{S} \boldsymbol{f} \in \mathbb{R}^{n\times3}$

can be defined as

$$\nabla_{\mathcal{S}} f = \frac{\partial f}{\partial \xi_\alpha} \otimes \boldsymbol{a}^\alpha = \nabla_\omega f \mathbf{J}^\dagger, \tag{4}$$

which yields the directional derivative on the surface when multiplied with some direction in $\mathbb{R}^3$ [SBS23]. Accordingly, we see that $\mathbf{J}\mathbf{J}^\dagger = \nabla_{\mathcal{S}} \boldsymbol{m}_0$ is the surface gradient of the rest state embedding, which is sometimes referred to as the "first fundamental tensor" $\mathbf{a}$ of the surface [BGMN19]. For a visualization of the involved maps, see Figure 3.

Deformation gradient Let $\mathbf{j} = \nabla_\omega \boldsymbol{m} \in \mathbb{R}^{3\times 2}$ denote the Jacobian of the embedding of the shell in some deformed state. Then, the deformation gradient $\mathbf{F} \in \mathbb{R}^{3\times 3}$ is given by

$$\mathbf{F} = \nabla_{\mathcal{S}} \boldsymbol{m} = \frac{\partial \boldsymbol{m}}{\partial \xi_\alpha} \otimes \boldsymbol{a}^\alpha = \mathbf{j}\mathbf{J}^\dagger. \tag{5}$$

Note the similarity of this to the expression to the deformation gradient of volumetric deformables in the context of FEM, where the Jacobians would be the element Jacobian in the reference and the deformed configuration, respectively — only here, the inverse is replaced by the pseudoinverse.

Microrotations Every point in a micropolar continuum has an orientation that is often identified by a set of pairwise orthonormal directors $\{\boldsymbol{d}_1, \boldsymbol{d}_2, \boldsymbol{d}_3\} \subset \mathbb{R}^3$. The directors can be interpreted as the columns of a rotation matrix $\overline{\mathbf{R}} = \boldsymbol{d}_i \otimes \boldsymbol{e}_i$, which is one possible representation of the previously introduced microrotation field. However, for the strain and stress in a micropolar material, the absolute orientation of the directors is not relevant, only the incremental rotation from the the rest state contributes to stresses. Therefore, the strain measures that we introduce below will only depend on the *elastic microrotation* $\mathbf{Q} \in SO(3)$ which is the rotation that maps the rest state microrotation $\overline{\mathbf{R}}_0$ to the total microrotation $\overline{\mathbf{R}}$:

$$\overline{\mathbf{R}} = \mathbf{Q}\overline{\mathbf{R}}_0 \quad \Leftrightarrow \quad \mathbf{Q} = \overline{\mathbf{R}}\,\overline{\mathbf{R}}_0^T. \tag{6}$$

Therefore, if the shell is in this rest state, the microrotation degrees of freedom would be $\mathbf{Q} = \mathbb{1}$. The rest rotation $\overline{\mathbf{R}}_0$ itself does not occur in any of the kinematic relations or constitutive laws, so we could leave it undefined. However, for example for an intuitive visualization of the director field, a common way to define the rest rotations is by the polar decomposition

$$\overline{\mathbf{R}}_0 = \mathrm{polar}[\boldsymbol{a}_1|\boldsymbol{a}_2|\boldsymbol{n}_0], \tag{7}$$

which results in a set of directors $\overline{\mathbf{R}}_0 = \boldsymbol{D}_i \otimes \boldsymbol{e}_i$ with $\boldsymbol{D}_3 = \boldsymbol{n}_0$ and the remaining directors tangent to the shell surface. The deformed third director $\boldsymbol{d}_3$ is always given by $\boldsymbol{d}_3 = \mathbf{Q}\boldsymbol{n}_0$. Note that in practice, after applying a discretization, the total microrotation $\overline{\mathbf{R}}$ is not continuous across elements (just as the discrete deformation gradient and macroscopic rotation $\mathbf{R}$ are not continuous in classical elasticity) as typical elements are not globally C^1 continuous. Therefore, $\overline{\mathbf{R}}$ is not uniquely defined on the edges or vertices of a discretization but it can be evaluated for example at the quadrature points. This does not apply to the elastic microrotation $\mathbf{Q}$ which is continuous between elements for conforming discretizations.

Strain measures The in-plane stretching and shearing of the shell is measured with the shell *strain tensor* $\overline{\mathbf{E}} \in \mathbb{R}^{3\times 3}$ given by

$$\overline{\mathbf{E}} = \mathbf{Q}^T\mathbf{F} - \mathbf{F}_0, \quad \text{with} \quad \mathbf{F}_0 = \mathbf{J}\mathbf{J}^\dagger, \tag{8}$$

which is the analogue to the three-dimensional Cosserat strain tensor $\overline{\mathbf{E}} = \overline{\mathbf{R}}^T\mathbf{F} - \mathbb{1}$, notably with the identity matrix replaced by the previously introduced surface identity tensor $\mathbf{J}\mathbf{J}^\dagger$. The strain due to spatially varying elastic microrotations is measured using the shell *curvature-bending tensor* $\boldsymbol{\Gamma} \in \mathbb{R}^{3\times 3}$ which is reminiscent of the "wryness tensor" as its three-dimensional counterpart:

$$\boldsymbol{\Gamma} = \mathrm{axl}\left(\mathbf{Q}^T \frac{\partial \mathbf{Q}}{\partial \xi_\alpha}\right) \otimes \boldsymbol{a}^\alpha = \boldsymbol{\Gamma}_\omega \mathbf{J}^\dagger, \tag{9}$$

where the columns of the matrix $\boldsymbol{\Gamma}_\omega \in \mathbb{R}^{3\times 2}$ are given by the axial vector terms from the first expression.

For both strain measures it can be shown that they are frame-independent (i.e. unaffected by rigid body transformations of the degrees of freedom), as well as independent of the local coordinates (i.e. independent of the parametrization) [NSBN23]. The independence from the parametrization is what allows the FEM discretization to directly use the local coordinates of the reference elements as a local parametrization. These local coordinates might be arbitrarily oriented relative to neighboring elements depending on node ordering. Due to the parametrization independence, this does not affect the energy of the shell. The strain measures are planar tensors (i.e. of rank 2) and their components measure the strain or curvature in the (possibly curved) reference configuration of the shell w.r.t. the cartesian basis of $\mathbb{R}^3$. For example, for a plate initially perpendicular to the z-axis, the third column of the strain measures will always be zero (i.e. no change in z-direction), while for a cylinder extending along the z-axis those entries will be non-zero if it is e.g. stretched in z-direction or twisted around the z-axis.

Non-Euclidean shells Although we do not know of a rigorously derived Cosserat shell model that explicitly incorporates non-Euclidean elasticity [SE10; CSvRV18], we can model similar effects using a modified "rest state" deformation gradient $\mathbf{F}_0$ or a "rest state" curvature tensor $\boldsymbol{\Gamma}_0$ by substituting $\overline{\boldsymbol{\Gamma}} = \boldsymbol{\Gamma} - \boldsymbol{\Gamma}_0$ in the constitutive model. As noted before, these rest quantities are defined with respect to the reference configuration in the cartesian basis of $\mathbb{R}^3$ — otherwise, if a different coordinate system is more convenient to prescribe the quantity, applying a change of basis to $\mathbb{R}^3$ is required. In our experiments in Section 5 we demonstrate several cases where this approach is used to generate complex deformations and shapes.

3.2. Constitutive model

A Cosserat material model for shells can be defined in terms of an energy density function Ψ depending on the previously introduced strain tensor $\overline{\mathbf{E}}(\mathbf{Q}, \mathbf{F})$ and the curvature tensor $\boldsymbol{\Gamma}(\mathbf{Q}, \partial\mathbf{Q}/\partial\xi_\alpha)$. In this work, we mainly focus on a Cosserat material model intended for plates (i.e. planar rest configurations), originally derived using dimensional reduction from a three-dimensional model by Neff [Nef04]. While this model is formally "exact" only for shells with planar rest configurations, we will also apply it to curved shells and experimentally verify our results by comparing it to a full Cosserat shell model for curved configurations. This reference model was rigorously derived by Bîrsan et al. [BGMN19] and extended for non-orientable surfaces by Nebel et al. [NSBN23]. It contains higher-order terms that make it accurate up to order $O(h^5)$ for

curved shells. For reference, we reproduce the variant of this curved shell model that we implemented for verification in the supplementary document. It also depends on additional expressions for rest state curvature measures (Gaussian curvature, mean curvature, etc.) which can be found in the supplementary document as well. Both models were derived such that the integration in thickness direction h was resolved analytically. In the case of planar rest geometries the curved shell model reduces exactly to the aforementioned plate model as all higher-order corrective terms are scaled by curvature measures of the rest geometry. Overall, these additional terms make the material slightly stiffer or softer in regions of high curvature. Therefore, applying the plate model to a curved rest configuration can be considered an approximation of the true material behavior. Our motivation for suggesting this approximation is that the plate model is cheaper to evaluate and easier to implement as the full shell model requires implementation of additional geometric curvature measures and it directly couples the strain measures in the constitutive model making the resulting derivatives significantly more complex. Finally, we note that while both models lead to a codimensional simulation in terms of the midfsurface, it is still possible to recover the full three-dimensional deformation including changes in thickness. Such reconstruction formulas can be found in the literature for the respective model [SNB16; NSBN23].

The Cosserat plate model We now give a brief overview of the Cosserat model for flat plates [Nef04; SNB16] that we employ. As introduced before, it can either be derived by dimensional reduction from a three-dimensional Cosserat deformable or by simplifying the curved shell model by assuming a flat reference configuration which removes all terms of order h^5 such that only terms of at most order h^3 remain. For a full derivation, we refer to the mechanics literature. After either of these procedures, the resulting internal energy of a Cosserat plate with thickness h can be written as

$$E(\overline{\mathbf{E}}, \boldsymbol{\Gamma}) = \int_\omega h\Psi_{\text{memb}}(\overline{\mathbf{E}}) + \frac{h^3}{12}\Psi_{\text{bend}}(\mathbf{c}\boldsymbol{\Gamma}) + h\Psi_{\text{curv}}(\boldsymbol{\Gamma})\, d\mathcal{S}, \quad (10)$$

where the "alternator tensor" $\mathbf{c} \in \mathbb{R}^{3\times3}$ is given by

$$\mathbf{c} = \left(\sqrt{\det \mathbf{I}}\right)^{-1} (\boldsymbol{a}_1 \otimes \boldsymbol{a}_2 - \boldsymbol{a}_2 \otimes \boldsymbol{a}_1), \quad (11)$$

and the first fundamental form $\mathbf{I} = \mathbf{J}^T\mathbf{J}$. The individual terms of Eq. (10) are the membrane energy density Ψ_{memb}, the bending energy density Ψ_{bend} and the Cosserat curvature energy density Ψ_{curv} which we discuss in the following sections.

Membrane energy The Cosserat membrane energy Ψ_{memb} determines the plate's response to in-plane stretching and shearing as well as the coupling of the displacement to the microrotation field. With the kinematic relations defined above, the "physically linear" (i.e. large rotation but small strain) isotropic membrane energy for a Cosserat plate is given by

$$\Psi_{\text{memb}}(\overline{\mathbf{E}}) = \mu\|\operatorname{sym}\overline{\mathbf{E}}\|_F^2 + \mu_c\|\operatorname{skew}\overline{\mathbf{E}}\|_F^2 + \frac{\mu\lambda}{2\mu+\lambda}\operatorname{tr}(\overline{\mathbf{E}})^2, \quad (12)$$

where μ and λ are the first and second Lamé parameters and μ_c is the Cosserat couple modulus. The formulation of the membrane energy is nearly identical to the energy of a three-dimensional micropolar model but is evaluated with the planar shell strain tensor instead. The couple modulus μ_c, which is introduced in addition to the parameters of classic linear elasticity, can be interpreted to control the coupling of the microrotations to the macroscopic rotation of the surface (as it penalizes the skew-symmetry part of the strain). Therefore, it was argued in the context of three-dimensional deformables in physically-based animation to use a value close to the stiffness of the material, i.e. $\mu_c \approx \mu$ [LFJ*23]. This avoids typical artifacts of linear materials that can appear if the microrotations could strongly deviate from the continuum. From a theoretical point of view, the Cosserat model can be seen as a generalization of the classic shear-rigid Kirchhoff-Love shells and shear-deformable Reissner-Mindlin plate models [Nef04] which can be recovered at the limits $\mu_c \to \infty$ and $\mu_c = 0$, respectively. However, these limit cases are numerically more challenging, requiring additional considerations. Similar to the three-dimensional model, the membrane energy can also be extended for large strains by replacing the linearized volume term $\operatorname{tr}(\overline{\mathbf{E}})^2$ with a nonlinear term such as

$$\Psi_{\text{V,nonlin}}(J) = \frac{1}{2}\left((J-1)^2 + (J^{-1}-1)^2\right), \quad J = \frac{\sqrt{\det \mathbf{i}}}{\sqrt{\det \mathbf{I}}}, \quad (13)$$

where J measures the local change in area with the first fundamental form $\mathbf{i} = \mathbf{j}^T\mathbf{j}$ in the deformed configuration.

Bending energy The bending energy Ψ_{bend} results from the dimensional reduction of a three-dimensional solid to a two dimensional surface and models its flexural stiffness due to the non-zero thickness. For the models we employ, the bending energy density is identical to the physically linear membrane energy density, i.e. $\Psi_{\text{bend}}(\mathbf{A}) := \Psi_{\text{memb}}(\mathbf{A})$ for some argument $\mathbf{A}$. As noted by Wen and Barbič [WB23], explicitly identifying the terms related to bending allows us to potentially scale the bending stiffness independently of the thickness in a non-physical way.

Curvature energy The curvature energy Ψ_{curv} is a purely non-classical contribution and can be used to introduce additional stiffness against changes of orientation of the microrotation field on top of the volumetrically-consistent bending energy. In this work, we consider the energy

$$\Psi_{\text{curv}}(\boldsymbol{\Gamma}) = \mu L_c^2\|\boldsymbol{\Gamma}\|_F^2, \quad (14)$$

where L_c is a characteristic length scale of a "microstructure" in the context of micropolar materials in the mechanics literature. For us however, this parameter and this term of the material model is mainly interesting to control the stiffness with respect to a prescribed "rest" curvature $\boldsymbol{\Gamma}_0$ independently of the thickness or stretching stiffness of the shell. We demonstrate this in our experiments in Section 5.

4. Problem formulation and discretization

After introducing the material model, we now present our discretization approach for the simulation of three-director Cosserat shells. Naturally, this procedure is slightly more involved than the discretization of classic shell or cloth models established in physically-based animation. While the mechanics and applied mathematics literature predominantly focuses on static problems,

we are mostly interested in the dynamic behavior of shells. In general, we build upon the approach for the discretization of micropolar volumetric deformables introduced by Löschner et al. [LFJ*23]. In summary, this includes the formulation of the dynamics as an incremental potential, spatial discretization using FEM and interpolation of the microrotation field by updating rotations at the quadrature points with interpolated angular velocities. We briefly recap the most important aspects and highlight the differences when adapting the approach to shells.

4.1. Incremental potential formulation

The foundation of our discretization is the implicit time integration of the shell model which we formulate as an optimization problem. We define its degrees of freedom to be the global translational and angular velocities $\boldsymbol{v}$ and $\boldsymbol{\omega}$ associated with the previously introduced material model. In particular, applying the backward Euler method, we solve for a minimizer of the incremental potential

$$E(\boldsymbol{v},\boldsymbol{\omega}) = E_{\text{int}}(\boldsymbol{v},\boldsymbol{\omega}) + E_{\text{ext}}(\boldsymbol{v},\boldsymbol{\omega}) + \frac{1}{2}(\boldsymbol{v}-\boldsymbol{v}_0)^T\mathbf{M}_\rho(\boldsymbol{v}-\boldsymbol{v}_0) + \frac{1}{2}(\boldsymbol{\omega}-\boldsymbol{\omega}_0)^T\mathbf{M}_j(\boldsymbol{\omega}-\boldsymbol{\omega}_0), \quad (15)$$

where E_{int} is the material's total strain energy, E_{ext} accounts for external potentials (such as gravity or contact potentials), $\boldsymbol{v}_0$ and $\boldsymbol{\omega}_0$ are the velocities at the end of the previous time step and $\mathbf{M}_\rho$ and $\mathbf{M}_j$ are the mass matrices for the translational and rotational degrees of freedom. Both matrices can either be lumped or computed in an FEM consistent way, taking into account a curved rest geometry as suggested by Wen and Barbič [WB23]. In practice, we assume a quasi-static behavior of the microrotation field by setting the rotational inertia density to zero ($\mathbf{M}_j = 0$). Although our formulation still permits using a non-zero value, doing so can cause unintuitive dynamic behavior as it assigns rotational inertia energy to individual material points. For example, consider a pendulum modeled with the present shell model and a non-zero rotational inertia density. When set into motion under gravity, this would cause the pendulum to accelerate more slowly as any initial potential energy will be converted not only into classical kinetic energy (i.e. a swinging motion) but instead split between the classical kinetic energy and the additional rotational inertia energy. While this could be desired behavior in the mechanics or engineering communities where micropolar materials are used in specialized applications, we consider this too obscure to explore in this work.

In order to robustly minimize the potential $E(\boldsymbol{v},\boldsymbol{\omega})$ we use Newton's method which requires the global gradient and Hessian of the objective function. We obtain the corresponding per-element derivative expressions using the symbolic differentiation framework SymX [FLW*23]. Overall, the optimization-based formulation allows us to easily couple the shell model with other physical systems, such as rigid bodies, volumetric (micropolar or classic) deformables or to incorporate a robust model for frictional contact such as IPC [LFS*20; LKJ21], by adding their respective energy contributions to the objective function. This also includes boundary conditions for positions or velocities and rotations or angular velocities which we prescribe using potentials corresponding to penalty forces. Even though it is possible to prescribe boundary conditions for the rotations (e.g. for "clamping" a surface using only its boundary nodes) this is not necessary to obtain a well-defined problem (at least in the case of $\mu_c > 0$).

4.2. Finite element discretization

For the spatial discretization of the model we use the finite element method. As established before, the surface of the shell has to be covered by patches of local parametrizations. When using FEM, this is realized through the tesselation of the surface into individual elements locally parametrized by their reference element. Referring back to the introduction of the kinematic relations, the configuration of the shell's rest state is described by the midsurface embedding $\boldsymbol{m}_0$. Its FEM interpolation inside of an element, parametrized by the reference element coordinates $\boldsymbol{\xi} \in \mathbb{R}^2$, is given by

$$\boldsymbol{m}_0(\boldsymbol{\xi}) = \sum_{i=1}^{n_{\text{sh}}} \boldsymbol{X}_i N_i(\boldsymbol{\xi}), \quad (16)$$

where $\boldsymbol{X}_i$ are the nodal positions in the undeformed configuration and $N_i(\boldsymbol{\xi}), i = 1,...,n_{\text{sh}}$ are the shape functions of the element. Then, the element Jacobian $\mathbf{J} \in \mathbb{R}^{3\times 2}$ is given by

$$\mathbf{J}(\boldsymbol{\xi}) = \frac{\partial \boldsymbol{m}_0}{\partial \boldsymbol{\xi}} = \sum_{i=1}^{n_{\text{sh}}} \boldsymbol{X}_i \nabla N_i(\boldsymbol{\xi}). \quad (17)$$

Both expressions can be written in terms of matrix multiplications

$$\boldsymbol{m}_0(\boldsymbol{\xi}) = \mathbf{X}^e \boldsymbol{N}^e(\boldsymbol{\xi}) \quad \text{and} \quad \mathbf{J}(\boldsymbol{\xi}) = \mathbf{X}^e \nabla \boldsymbol{N}^e(\boldsymbol{\xi}), \quad (18)$$

where $\mathbf{X}^e \in \mathbb{R}^{3\times n_{\text{sh}}}$ is the horizontally stacked vector of nodal positions, $\boldsymbol{N}^e(\boldsymbol{\xi}) \in \mathbb{R}^{n_{\text{sh}}}$ is the column vector of the element's shape functions and $\nabla \boldsymbol{N}^e(\boldsymbol{\xi}) \in \mathbb{R}^{n_{\text{sh}}\times 2}$ is the corresponding Jacobian. Following these definitions we can directly evaluate, e.g., the deformation gradient $\mathbf{F} = \mathbf{j}\mathbf{J}^\dagger$ with $\mathbf{j} = \mathbf{x}^e \nabla \boldsymbol{N}^e$. The other kinematic quantities follow accordingly. The evaluation of the total strain energy is then approximated using numerical integration over n_{el} elements with a quadrature rule on the reference element with n_{qp} points by

$$E_{\text{int}} = \int_\omega \Psi d\mathcal{S} \approx \sum_i^{n_{\text{el}}} \int_{\hat{T}} \Psi(\boldsymbol{m}_0(\boldsymbol{\xi}))\sqrt{\det \mathbf{I}_i(\boldsymbol{\xi})}\, d\boldsymbol{\xi} \quad (19)$$

$$\approx \sum_i^{n_{\text{el}}} \sum_j^{n_{\text{qp}}} \hat{w}_j \hat{\Psi}(\hat{\boldsymbol{p}}_j)\sqrt{\det \mathbf{I}_i(\hat{\boldsymbol{p}}_j)}\, d\boldsymbol{\xi}, \quad (20)$$

where $\hat{T}$ is the reference element, $\mathbf{I}_i(\boldsymbol{\xi}) = \mathbf{J}_i(\boldsymbol{\xi})^T\mathbf{J}_i(\boldsymbol{\xi})$ is the first fundamental form of the i-th element, $\hat{w}_j$ and $\hat{\boldsymbol{p}}_j$ are the weights and points of a quadrature rule and $\hat{\Psi}$ is strain energy density transformed to the the reference element.

Interpolation of rotations To numerically integrate the energy density over an element according to Eq. (20), the embedding of the deformed shell $\boldsymbol{m}$ and the microrotation field $\mathbf{Q}$ has to be evaluated at the quadrature points. The deformation of the shell can be interpolated analogous to Eq. (16). As we use velocities as degrees of freedom, we additionally have to substitute the time integration rule into the interpolation to obtain the updated nodal positions of the current configuration. For the microrotation field however, it is

less clear how to obtain a consistent interpolation scheme as rotations do not form a vector space. We follow the approach introduced by Löschner et al. [LFJ*23] which keeps track of the rotations at the quadrature points as additional history variables and updates them by applying a time integration rule for quaternions, either exactly using the quaternion exponential function or using the common approximation

$$\boldsymbol{q}(\omega) \approx \frac{\tilde{\boldsymbol{q}}(\omega)}{\|\tilde{\boldsymbol{q}}(\omega)\|} \quad \text{with} \quad \tilde{\boldsymbol{q}}(\omega) = \boldsymbol{q}_0 + \frac{\Delta t}{2}\omega_q \boldsymbol{q}_0, \tag{21}$$

where ω_q is a quaternion with its imaginary part set to the angular velocity which can be interpolated as a vector from the nodal values. This is done in each Newton iteration as part of the energy evaluation. To get rid of a potential path dependence of the solution due to the additional history variables, the incrementally updated rotations could be "reset" after each or a certain number of time steps, for example using the stable updating approach proposed by Magisano et al. [MLMG20] or using spherical weighted averages [BF01]. In our experiments however, this was not necessary even for time step sizes around $\Delta t = 10\,\text{ms}$. The orientation of the directors (i.e. columns of the rotation matrix $\mathbf{Q}$) can be recovered by converting the quaternion $\boldsymbol{q}$ into its matrix representation.

Curvature tensor from quaternions Above, the curvature tensor $\boldsymbol{\Gamma}$ was introduced in terms of the rotation matrix representation $\mathbf{Q}$ of the elastic microrotations. As we use a unit quaternion representation $\boldsymbol{q}$ in practice to perform the time integration, we directly compute the curvature tensor based on unit quaternions by

$$\boldsymbol{\Gamma} = \boldsymbol{\Gamma}_\omega \mathbf{J}^\dagger \quad \text{with} \quad \boldsymbol{\Gamma}_\omega = 2\,\text{vec}\left(\text{conj}(\boldsymbol{q})\frac{\partial \boldsymbol{q}}{\partial \xi_\alpha}\right) \otimes \boldsymbol{e}_\alpha, \tag{22}$$

where $\text{vec}(\boldsymbol{q}) \in \mathbb{R}^3$ denotes the imaginary part of the quaternion, $\text{conj}(\boldsymbol{q})$ its conjugate and $\boldsymbol{e}_\alpha$ are the unit vectors of $\mathbb{R}^2$. The gradient of $\boldsymbol{q}$ is approximated analogous to Eq. (17).

Quadrature rules and element type As the interpolation of the nodal rotations to the interior of an element is nonlinear (which all consistent interpolation approaches have in common), a single quadrature point is generally not enough to accurately integrate the involved energy densities even on linear elements. This is in contrast to classic elasticity where a single quadrature point is sufficient for linear elements due to the constant deformation gradient. More specifically, using only one quadrature point can be considered a form of reduced integration in the context of the Cosserat model. With this approach we encountered numerical artifacts such as zero-energy modes in the rotation field making this choice basically unusable without further modifications.

However, seemingly unlike to the three-dimensional model, using more accurate quadrature rules for linear elements lead to significant locking issues for shells. This prevents the simulation especially of stiff but bendable materials without excessively fine meshes. In the context of shells, locking is a well known problem in engineering [HLP96], applied mathematics [Wei12; Qua12] and computer graphics [LKJ21; LDB*23]. We note that the results from Weischedel [Wei12] for one-director Cosserat shells can not be trivially applied to the Cosserat model presented here, as our degrees of freedom include an entire frame of directors instead of only one director. A mid-edge discretization of the microrotation field (corresponding to non-conforming Crouzeix–Raviart elements) does not seem to be sufficient to resolve locking.

To alleviate the issue for our implementation of the three-director Cosserat model, we follow the conclusions of Sander et al. [SNB16] and Nebel et al. [NSBN23] that a second-order discretization of the deformation combined with a first-order discretization of the rotation field should be appropriate to resolve locking in most cases. In particular, we will employ second-order Lagrange triangles (quadratic, six nodes) for the deformation, combined with standard first-order Lagrange triangles (linear, three nodes) for the rotation. As the geometry of the shell and accordingly the shape of the elements is defined by the quadratic elements, the element Jacobian is always provided by the quadratic element, even for the evaluation of the rotation gradients. The basis functions of the linear elements are only used for the interpolation of the angular velocities and rotation gradients and they can reuse the connectivity of the quadratic mesh (by ignoring the edge midpoints). For the numerical integration we use a three-point Gaussian quadrature rule of order two for all triangle elements (see supplementary document) We performed several experiments (see Section 5.1) to validate that our implementation of the discretization is mostly locking free.

5. Evaluation

In the following, we present several experiments to check the correctness of our implementation, to verify the consistency of the model and the discretization and to demonstrate applications of the Cosserat shell model in the context of physically-based animation. For strong coupling with existing physical models, we used the STARK simulation framework [FLL*24]. We always initialize the elastic microrotation field $\mathbf{Q}$ (or rather the corresponding quaternions) with an identity rotation as we reasoned in Section 3.1. All experiments use second-order Lagrangian triangle elements (later denoted as quadratic elements), as reasoned in Section 4.2, except for comparisons where a differing element type is explicitly noted. This information, including full timing information and the number of the corresponding degrees of freedom for all experiments, can also be found in in the supplementary document. All timings were measured on a workstation with an AMD 5975WX CPU (32 cores, 3.6 GHz) and 256 GB of DDR4 8-channel RAM. To render quadratic triangle meshes, we use the quadratic basis functions to interpolate displacements and normals onto a finer linear triangle mesh obtained by subdivision of the simulation mesh at rest.

System solves For the solution of the linear system in each Newton iteration we generally use a direct solver based on LU decomposition. Employing a direct solver guarantees robust solves even for extremely stiff material parameters and challenging contact problems. As for classic hyperelastic material models, the Hessian of the Cosserat shell model can generally become indefinite even in simple scenarios such as the twisting strip shown in Figure 4. However, for scenarios which are dominated by elastic forces (without contact and friction), a simple numerical projection to positive definiteness of element-wise Hessians often leads to a substantial increase in the number of iterations required for Newton's method to converge (similar to classic materials [LLF*23]). Therefore, we

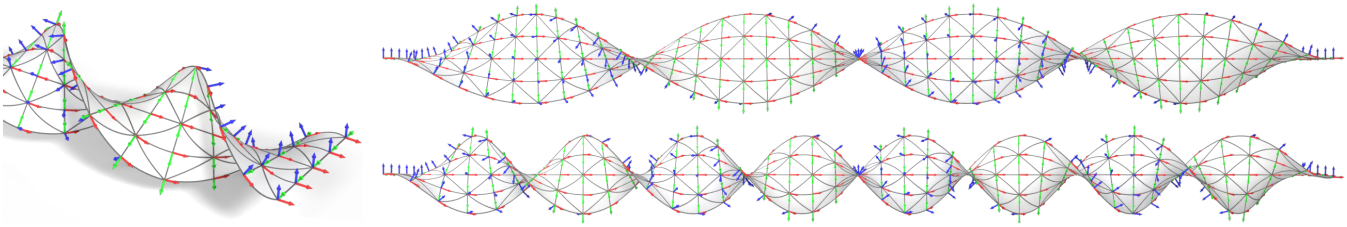

Figure 4: *A clamped plate is twisted by two (top right) and four full revolutions (bottom right) with an angular velocity of one revolution per second. The elastic microrotation field* $\mathbf{Q}$ *is visualized using a coordinate frame oriented according to its columns (the directors). As the initial configuration is flat, they coincide with the total microrotation* $\overline{\mathbf{R}}$ *and the z-axis (blue) is almost perpendicular to the surface.*

opted to not perform projections of the shell model at all and to only project contributions of the contact model. Finally, while the LU decomposition is a safe choice to solve even indefinite systems, this can in principle result in a direction that is not a descent direction. In these situations we restart the time step with a smaller step size which happened only for some challenging contact situations in our experiments and did not occur in the purely elastic experiments. Nevertheless, for applications with strong robustness requirements, even in degenerate configurations, further analysis regarding inversion stability and projections should be performed in the future. For experiments with very stiff materials, we implement the robust line search method introduced by Longva et al. [LLF*23]. To determine convergence of Newton's method, we use the residual of the balance of forces and for most experiments we apply a tolerance of $\epsilon = 1 \cdot 10^{-7}$ on the maximum norm. For experiments with frictional contact we use a tolerance of $\epsilon = 1 \cdot 10^{-3}$.

Contacts In our experiments, we demonstrate interactions of micropolar shells with our implementation of IPC [LFS*20]. For the contact handling of the quadratic surface meshes we obtain a collision proxy mesh by performing a trivial subdivision per quadratic triangle into four linear triangles, directly reusing the existing mesh vertices without additional interpolation. This corresponds to the most simple realization of the "High-Order IPC" concept introduced by Ferguson et al. [FJZ*23]. For more details on contact handling we refer to the course by Andrews et al. [AEF22].

Constitutive model We presented two Cosserat models, a simplified plate model for planar rest configurations (Section 3.2) and a shell model specifically for curved initial configurations (see supplementary document). If not otherwise indicated, we used the plate model for the following experiments. In particular, for geometries with an actually planar rest state the curved shell model is identical to the plate model as all additional terms vanish for zero rest state curvature. In the "Möbius strip" and "twisted half sphere" experiments described below (see Section 5.3), we compare both models on actual curved geometry to justify our application of the plate model, even for non-planar piecewise affine meshes.

5.1. Validation: discretization and locking

Twisting strip To verify that our discretization of the Cosserat shell model can handle large rotations, we simulate a plate (10 cm × 1 cm, $h = 2$ mm) clamped on one side. The plate is very stiff (parameters based on aluminum) without significant additional bending stiffness ($E = 7 \cdot 10^{10}$ Pa, $\nu = 0.35$, $\mu_c = \mu$, $L_c = 2 \cdot 10^{-6}$ m). On the non-clamped side, we prescribe a constant twisting angular velocity of $\omega_x = 360\,°\,\mathrm{s}^{-1}$ to both the nodal positions and rotations over 4 s with a fixed time step of $\Delta t = 10$ ms. As shown in Figure 4, this set of parameters leads to an almost symmetricly twisted configuration with four complete twists of the plate without any inversions or buckling. At this final configuration, the maximum angular distance between orientations inside of an element over the entire mesh is 51.7°. Newton's method required on average 4 iterations per time step to converge without any projection.

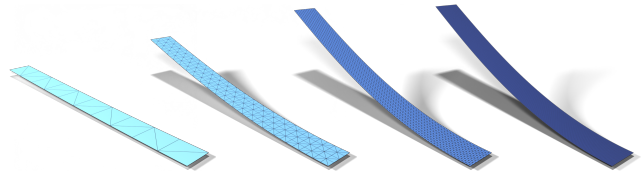

Final frame for linear triangle meshes ($n_y = 1, 4, 16, 64$)

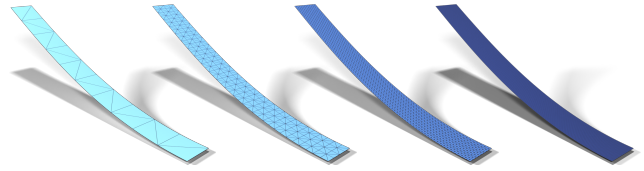

Final frame for quadratic triangle meshes ($n_y = 1, 4, 16, 64$)

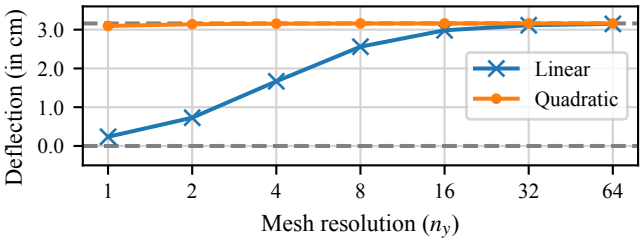

Figure 5: *We apply a progressive load to a plate which leads to different deflections depending on the discretization. The dashed lines indicate max. and min. expected deflection (i.e. solution of finest mesh vs. no deflection). Linear elements exhibit shear-locking while quadratic elements yield accurate results even for coarse meshes.*

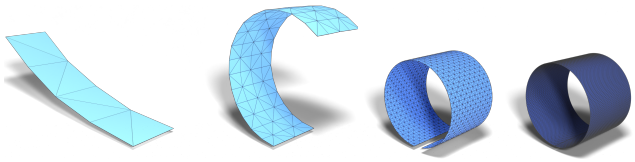

Final frame for linear triangle meshes ($n_y = 1, 4, 16, 64$)

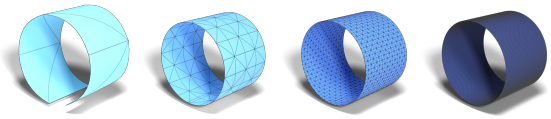

Final frame for quadratic triangle meshes ($n_y = 1, 4, 16, 64$)

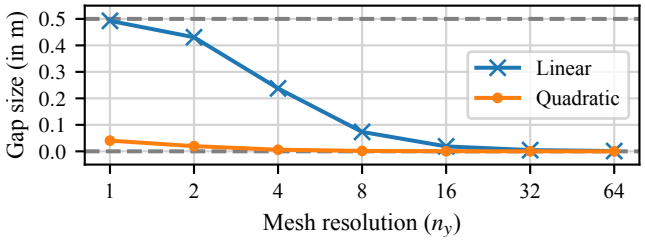

Figure 6: *For an initially flat plate ($L = 0.5\,\mathrm{m}$) we prescribe the curvature of a cylinder ($H = 1/r = 4\pi\,\mathrm{m}^{-1}$) which results in a near cylindrical shape with a gap between the plate's ends depending on the discretization. The dashed lines indicate the maximum and minium achievable gap size (i.e. plate length vs. zero gap). Again, quadratic elements converge very quickly.*

Plate under load To investigate locking, we repeat a classic experiment similar to the one performed by Sander et al. [SNB16]. We clamp a plate on one side, with the same parameters and dimensions from the twisting experiment. Along the edge of the free end, we apply a linearly increasing load of up to 50 N in the positive global z-direction. We perform the experiment with a sequence of meshes under uniform refinement, starting with $n_x \times n_y = 10 \times 1$ squares split into two triangles each. For the discretization we compare linear elements with quadratic elements for the displacement, while the rotations are always discretized using linear elements. For the evaluation, we measure the deflection of the free end of the plate which is visualized in Figure 5. It is clearly visible that linear elements exhibit locking which is not present if the displacement is discretized with quadratic elements. This behavior is not limited to extremely stiff materials as demonstrated here, but can also be observed for an appropriately scaled down stiffness and load.

Cylinder coiling As a variation on the previous experiment and to verify our implementation of the curvature tensor and the associated bending energy terms, we perform a second locking experiment. This time, we clamp an initially planar plate ($50\,\mathrm{cm} \times 12.5\,\mathrm{cm}$, $h = 1\,\mathrm{cm}$) of a softer material ($E = 1 \cdot 10^6\,\mathrm{Pa}$, $\nu = 0.35$; $\mu_c = \mu$, $L_c = 1 \cdot 10^{-2}\,\mathrm{m}$) on one side. Per quadrature point, we prescribe a rest-state curvature tensor $\mathbf{\Gamma}_0$ (see Section 3.1) with all entries set to zero except for $[\mathbf{\Gamma}_0]_{21} = 4\pi\,\mathrm{m}^{-1}$ which matches the curvature of a cylinder of the given dimensions. Again, we simulate a series of uniformly refined meshes starting with a grid of $n_x \times n_y = 4 \times 1$. For the evaluation, we measure the Hausdorff distance between the two ends of the plate which should ideally be zero when the plate forms a cylinder. As shown in Figure 6, with linear elements, the plate does not form a cylinder at all for coarse meshes, improving only after several levels of refinement. Whereas individual quadratic elements are also generally unable to perfectly reproduce a non-zero constant mean curvature (as polynomials do not have a constant radius of curvature), they already show a good approximation of the cylinder with the coarsest mesh.

The results of our two previous experiments regarding locking are in agreement with the conclusions drawn by Sander et al. [SNB16] and Nebel et al. [NSBN23] that for Cosserat shells second-order elements are necessary for the discretization of the displacement field to avoid substantial shear-locking while first-order elements are sufficient to discretize the rotations.

Regarding the runtime of simulations, it is clear that for a mesh with the same number of elements a simulation with quadratic elements will be slower due to the higher number of degrees of freedom which makes assembly and linear solves more costly. This is exacerbated with increasing mesh resolution due to the cubic complexity of the LU decomposition. However, if we compare simulations with comparable behavior, we can achieve a significant speedup with quadratic elements. For example, in our "plate under load" experiment for a grid of $n_y = 16$ elements, quadratic elements required 2.7 more runtime than linear elements (550 ms vs 201 ms per time step). However, a quadratic mesh with $n_y = 2$ performs already comparable to the linear mesh and runs 6.3 times faster (32 ms per time step) than the higher resolution linear mesh. For full timing information see the supplementary document.

5.2. Consistency with other models

Three-dimensional deformables To verify the consistency of the presented Cosserat shell model with its "parent" three-dimensional model (see e.g. [NBO15]), we recreate the "lotus flower" scene shown by Löschner et al. [LFJ*23] with identical material parameters but using codimensional shells. The material is relatively soft to stretching but stiff to bending ($E = 5 \cdot 10^5\,\mathrm{Pa}$, $\nu = 0.3$; $\mu_c = \mu$, $L_c = 1\,\mathrm{m}$). The three layers of the "flower" are plates ($1\,\mathrm{m} \times 1\,\mathrm{m}$, $h = 1\,\mathrm{cm}$), originally discretized by a $100 \times 100 \times 1$ hexahedral grid subdivided into linear tetrahedrons. Over time, a linearly increasing curvature is prescribed with a different strength per layer and a single vertex in the center is fixed in position. For the evaluation, we compare the final shape of the codimensional plates of different mesh resolutions to the three-dimensional model as rendered in Figure 7. For the error metric, we compute the maximum between the Hausdorff RMS (root mean square) distances of the midsurface of the volumetric mesh to the reduced model and vice versa, which is plotted in Figure 8. We observe that the shell model is visually already close to the volumetric solution for the coarsest resolutions and with refinement the distance quickly falls within the thickness of the plates. Although a more detailed analysis would require an even finer volumetric discretization, especially in the thickness direction, this generally confirms the consistency of the shell model.

Kirchhoff-Love shells In this experiment we qualitatively compare simulations of our implementation of the Cosserat shells

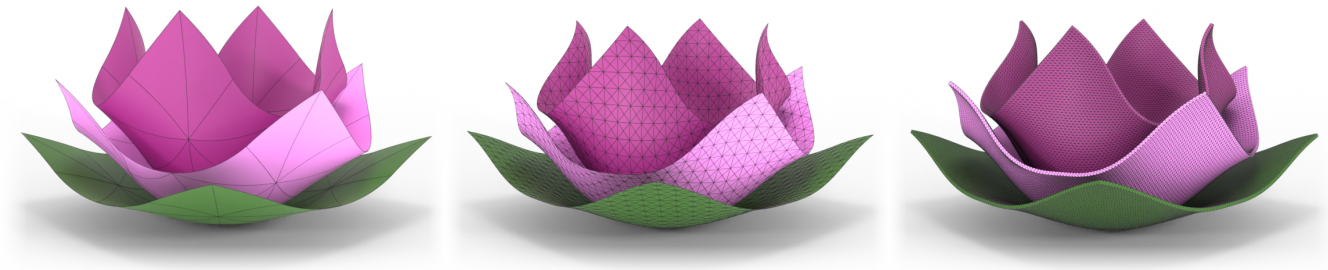

Figure 7: *We recreate the micropolar "lotus flower" scene [LFJ*23] with the codimensional shell model and identical material parameters. Even a coarse* 4×4 *grid of quadratic elements per layer matches the shape well (left), while the* 32×32 *grid matches the displacement almost perfectly (middle). Originally, the volumetric simulation used 60k linear tetrahedrons (*$100\times100\times1$ *grid, right). For the error between the codimensional simulations and the volumetric solution see Figure 8.*

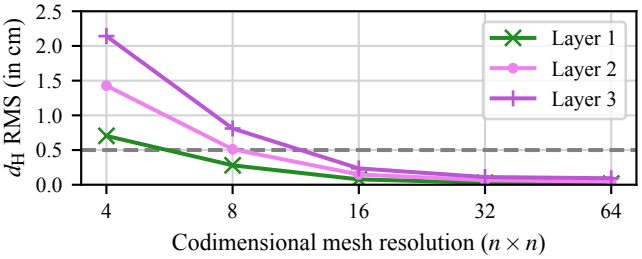

Figure 8: *The plot shows, per layer of the lotus flower (see Figure 7), the RMS of the Hausdorff distance* d_H *between the midsurface of the volumetric mesh (fixed resolution) and the shell model with increasing mesh resolution. The distance quickly falls within the plate's envelope* $(h/2$*, dashed line) and indicates consistency of the shell with the volumetric model.*

(quadratic elements) with an implementation of the Kirchhoff-Love shell model by Wen and Barbič [WB23] with a St. Venant-Kirchhoff material (linear elements). We simulate the Stanford bunny (scaled to 50 cm height) with three different shell thickness values ($h = 10$ mm, 3.75 mm and 1.5 mm) and a soft material ($E = 1\cdot10^5$ Pa, $\nu = 0.4$) under gravity ($\rho = 500\,\mathrm{kg\,m^{-3}}$), with frictional contact and with a clamped base. For the Cosserat shell we use the nonlinear volume term given by Eq. (13). While we cannot expect identical results, due to the fundamental difference in the models' assumptions, we obtain qualitatively similar dynamic behaviors of the shells as shown in Figure 9. Furthermore, we observed that the KL model can be more easily affected by very low quality meshes with stretched triangles and large differences in area. The discrete curvature measures and normal orientations used by it can strongly fluctuate between neighboring elements around sharp corners, leading to less stable contributions of the bending terms and more Newton iterations, especially for larger thickness values. Whereas we can circumvent this for the Cosserat model by approximating the shell's behavior with the simplified plate model which does not depend at all on the surface normals (bending and curvature terms only depend on the microrotation DOF), this is not possible for the KL model as bending is inherently defined by the normals. However, such problems were rare and did not occur for typical meshes of decent quality.

Figure 9: *Three bunnies of thickness* $h = 10$ mm, 3.75 mm *and* 1.5 mm *(left to right) simulated with the Cosserat plate model (top row) behave qualitatively consistent with the Kirchhoff-Love model with St.VK material presented by Wen and Barbič [WB23] (bottom row). The transparent shape indicates the rest shape.*

5.3. Controlled deformation

With the Cosserat shell model we have several ways of directly or indirectly influencing the rotational degrees of freedom and the curvature of a shell. This includes directly prescribing rotations or angular velocities as boundary conditions on nodes of the mesh, applying external angular accelerations or torques (as surface loads or volume densities) and manipulating the rest curvature of the shell.

Curvature "modes" To demonstrate the effects of prescribing different components of the curvature tensor by specifying a non-zero $\mathbf{\Gamma}_0$, we use a plate ($8\,\mathrm{cm}\times100\,\mathrm{cm}$, $h = 1$ cm) that is very soft to stretching but stiff to bending ($E = 1\cdot10^4$ Pa, $\nu = 0.3$; $\mu_c = \mu$, $L_c = 1$ m). A single row of vertices in the middle of the plate, parallel to its shorter extent, is fixed in position. Per simulation run, we prescribe for one entry of the curvature tensor a positive curvature on the right side of the boundary condition and the opposite curvature on the left. The results are visualized in Figure 10.

Acrobatic armadillos To show the effect of rest curvature on non-planar meshes, we repeat the previous experiment with three ar-

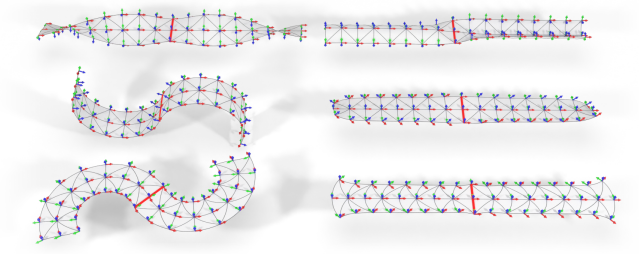

Figure 10: *Visualization of the different curvature "modes" by respectively prescribing one component of the rest curvature tensor $\mathbf{\Gamma}_0$ per plate. One row in the middle of each plate (red line) is fixed in position and we prescribe positive/negative curvature values to the right/left of it. We obtain four out-of-plane bending modes (two top rows) and two in-plane "drilling" modes (bottom row).*

Figure 11: *The curvature of these armadillos (non-planar shells) was prescribed by modifying the third column of the rest curvature tensor $\mathbf{\Gamma}_0$ corresponding to orientation changes along the z-axis. Individually prescribing a curvature value per row results in bending around the x-, y- or z-axis, respectively (left to right).*

madillos. For each of the deformed armadillos shown in Figure 11 we set a constant prescribed curvature along the global z-axis, i.e. the third column of the curvature tensor $\mathbf{\Gamma}_0$. This confirms the intuition we gave about the orientation of the strain measures given in Section 3.1. For a non-planar mesh, all entries of the curvature tensor $\mathbf{\Gamma} \in \mathbb{R}^{3\times3}$ may be non-zero, however it will always be of (column) rank 2 as it never has a component normal to the surface.

Buckling of a circular plate To demonstrate another aspect of non-Euclidean shells, we recreate an experiment of a circular plate with curved boundary ($r = 2.5\,\mathrm{cm}$, $h = 0.3\,\mathrm{mm}$, $E = 1 \cdot 10^6\,\mathrm{Pa}$, $\nu = 0.4$; $\mu_c = \mu$, $L_c = 1 \cdot 10^{-3} h$) subject to non-uniform growth,

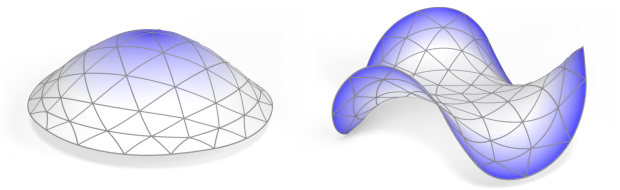

Figure 12: *The Cosserat shell model also allows us to prescribe a "rest" deformation gradient $\mathbf{F}_0$, here, a radially varying expansion (white: no expansion, blue: highest expansion) to reproduce the buckling of non-Euclidean shells shown by Chen et al. [CSvRV18].*

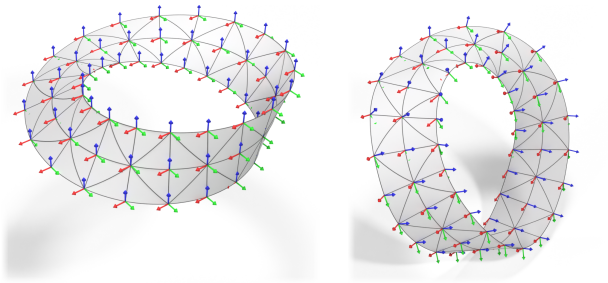

Figure 13: *A Möbius strip (80 curved second-order triangles) clamped on the top left side is subject to gravity. The coordinate frames visualize the elastic microrotation $\mathbf{Q}$ (the rotational degrees of freedom) which are given the identity matrix in the rest state (left). As the rest configuration is curved, the z-axis (blue) generally does not correspond to the (possibly sheared) surface normal given by the total microrotation $\overline{\mathbf{R}} = \mathbf{Q}\overline{\mathbf{R}}_0$ (see Section 3.1).*

discretized with 120 curved second-order triangles. To achieve this, we scale the actual rest value of $\mathbf{F}_0$ (see Eq. (8)) with a radially and time-dependent factor $c(r,t)$ of up to $c = 1.35$. At some point the expanded material "does not fit" into the planar shape constrained by the non-expanded material and buckles out-of-plane. Depending on whether the highest expansion is in the center or on the boundary of the plate, we obtain the shapes shown in Figure 12 which qualitatively agree with results from Chen et al. [CSvRV18].

Möbius strip As a first experiment to validate the use of the Cosserat plate model for the simulation of curved shells, we simulate a Möbius strip under gravity (inspired by [NSBN23]). To obtain a mesh with actually curved elements, we construct the Möbius strip in a preceding simulation where we twist and bend a plate ($10\,\mathrm{cm} \times 1\,\mathrm{cm}$, $h = 0.5\,\mathrm{mm}$) consisting of 80 second-order elements by prescribing curvature followed by a "merge by distance" operation when the two ends are close enough such that we obtain the final non-orientable surface. This mesh is then used as the rest state for the actual simulation ($E = 1 \cdot 10^6\,\mathrm{Pa}$, $\nu = 0.4$; $\mu_c = \mu$, $L_c = 1 \cdot 10^{-3} h$) with gravity ($\rho = 2000\,\mathrm{kg\,m^{-3}}$). For comparison, we ran the simulation with our two implemented Cosserat models (the plate and curved shell model, respectively, see Section 3.2). To determine the error between the models we measured the maximum two-sided Hausdorff distance between the surfaces at the end of the simulation which amounted to an absolute maximum distance of only $d_{\mathrm{abs}} = 7 \cdot 10^{-6}\,\mathrm{m}$ or a relative distance w.r.t. to the bounding box of the Möbius strip of $d_{\mathrm{rel}} = 1.56 \cdot 10^{-4}$. The two shells behaved visually identical through the simulation. Newton's method required on average 2 iterations to converge to our tolerance.

Twisted half sphere For the experiment shown Figure 1 (right), we simulate a half sphere with 1536 curved elements ($r = 1\,\mathrm{m}$, $h = 1\,\mathrm{mm}$) made from a soft material ($E = 1 \cdot 10^4\,\mathrm{Pa}$, $\nu = 0.4$; $\mu_c = \mu$, $L_c = 1 \cdot 10^{-5}\,\mathrm{m}$). Over the first 4 s of the simulation we directly apply an angular velocity of $\omega_z = 90^\circ\,\mathrm{s}^{-1}$ to a single vertex (the north-pole) of the half sphere while its equator is fixed in position. The prescribed angular velocity results in complex wrinkling and the shape shown in the render. The scene is simulated with fric-

tional contact to avoid obvious penetrations. As in the previous experiment, we compare the deformations of the shell at the end of the simulation obtained with the Cosserat plate and curved shell model, respectively. The maximum two-sided Hausdorff distance between the solutions was $d_{\text{abs}} = 1 \cdot 10^{-6}$ m or $d_{\text{rel}} = 1.4 \cdot 10^{-7}$ relative to the bounding box. Again there was no visual difference during the entire simulation. The runtime of this scene for 6 s simulated time was 126 s in total or 210 ms on average per time step with the plate model and 141 s in total or 234 ms on average per time step with the curved shell model. Overall the simulation with the shell model was approximately 12% slower, mostly due to the more expensive evaluation of the material model itself. Newton's method required on average 2-3 iterations to converge to our tolerance, largely unaffected by the choice of model.

Ancient papyrus scroll For this experiment we start with a "wrinkled" (non-planar) sheet of "papyrus" (0.5 m × 0.25 m, $h = 1$ mm) with a stiffer material ($E = 1 \cdot 10^8$ Pa, $\nu = 0.3$; $\mu_c = \mu$, $L_c = 1 \cdot 10^{-2}$ m) made of 200 curved second-order elements. Originating from the two shorter sides, we prescribe a spatially and temporally varying rest curvature $\boldsymbol{\Gamma}_0$ to roll it like a scroll. Afterwards, we add three rigid bodies with prescribed kinematics to push the scroll open again by frictional contact which results in the configuration shown in Figure 1 (left). Over 1509 time steps with an average $\Delta t = 9.9$ ms, Newton's method required on average 4-5 iterations to converge to our tolerance, however some time steps are significant outliers with many more iterations due to complex contacts. The runtime of this scene for 15 s simulated time was 272 s in total or 180 ms on average per time step.

6. Conclusion

In this work we proposed a novel incremental potential formulation of three-director Cosserat ("micropolar") shells well suited for the application in physically-based animation and allowing for strong coupling with frictional contact and other physical systems. We presented a corresponding FEM discretization for non-planar meshes with second-order elements which did not show significant locking in our experiments. In our evaluation, we also demonstrated that our formulation is quantitatively consistent with the three-dimensional Cosserat (micropolar) continuum model but requires much fewer degrees of freedom to achieve visually comparable results. Furthermore, we compared two existing constitutive models, a Cosserat model for curved shells and a simplified model for initially planar plates and found that the models yield comparable results on curved geometries. Therefore, we recommend the use of the plate model in the context of computer graphics as it is cheaper to evaluate and easier to implement because it does not depend on any geometric curvature measures and also has less complex derivatives as the strain measures do not get directly coupled as in the curved shell model. Additionally, it is worth noting that the low number of Newton iterations that were required for the model to converge to our residual tolerance indicate that the rotational degrees of freedom do not pose a significant numerical challenge relative to other established continuum-based shell models.

We also identified some interesting opportunities for future work in this direction. While we focused on three-director Cosserat models, a practical evaluation of one-director models in physically-based animation remains a compelling future avenue. Weischedel [Wei12] suggested a discretization of such a one-director model with linear triangles motivated by discrete differential geometry, however we also see applications for a higher-order discretizations to simulate curved geometries. Secondly, for practical applications where the robustness of the constitutive model is of high importance it would make sense to more thoroughly investigate the inversion stability [SHST12], robustness in demanding buckling scenarios and definiteness properties of the model in the spirit of recent work of Wu and Kim [WK23] and Shi and Kim [SK23] and similarly motivated works [SGK19]. For the temporal discretization, we applied first-order methods. Due to the rotational degrees of freedom, application of higher-order time integration methods [LLJ*20] remains an open problem for now. Finally, as we focused on an isotropic physically linear model with large rotations, it would be a logical next step to explore nonlinear and anisotropic constitutive models. Overall, we believe to have presented intriguing examples for the use of the additional modes of control that Cosserat models offer and we hope to inspire future research in this direction.

Acknowledgements

The armadillo and the bunny models are courtesy of the Stanford Computer Graphics Laboratory. This work is funded by the Deutsche Forschungsgemeinschaft (DFG, German Research Foundation) — 281466253. Open Access funding enabled and organized by Projekt DEAL.

References

[AAE10] Altenbach, Johannes, Altenbach, Holm, and Eremeyev, Victor A. "On generalized Cosserat-type theories of plates and shells: a short review and bibliography". *Archive of Applied Mechanics* 80.1 (Sept. 2010), 73–92. DOI: 10.1007/s00419-009-0365-3 3.

[AEF22] Andrews, Sheldon, Erleben, Kenny, and Ferguson, Zachary. "Contact and friction simulation for computer graphics". *ACM SIGGRAPH 2022 Courses*. SIGGRAPH '22. Aug. 2022. DOI: 10.1145/3532720.3535640 9.

[BC14] Bargteil, Adam W. and Cohen, Elaine. "Animation of Deformable Bodies with Quadratic Bézier Finite Elements". *ACM Transactions on Graphics* 33.3 (May 2014), 1–10. DOI: 10.1145/2567943 3.

[BD12] Bender, Jan and Deul, Crispin. "Efficient Cloth Simulation Using an Adaptive Finite Element Method". *Virtual Reality Interactions and Physical Simulations*. VRIPHYS '12. 2012. DOI: 10.2312/PE/VRIPHYS/VRIPHYS12/021-030 2.

[BF01] Buss, Samuel R. and Fillmore, Jay P. "Spherical averages and applications to spherical splines and interpolation". *ACM Transactions on Graphics* 20.2 (Apr. 2001), 95–126. DOI: 10.1145/502122.502124 8.

[BGMN19] Bîrsan, Mircea, Ghiba, Ionel-Dumitrel, Martin, Robert J, and Neff, Patrizio. "Refined dimensional reduction for isotropic elastic Cosserat shells with initial curvature". *Mathematics and Mechanics of Solids* 24.12 (July 2019), 4000–4019. DOI: 10.1177/1081286519856061 3, 5.

[BMF03] Bridson, Robert, Marino, Sebastian, and Fedkiw, Ronald. "Simulation of Clothing with Folds and Wrinkles". *ACM SIGGRAPH/Eurographics Symposium on Computer Animation*. SCA '03. 2003, 28–36 1–3.

[BMWG07] BERGOU, MIKLÓS, MATHUR, SAURABH, WARDETZKY, MAX, and GRINSPUN, EITAN. "TRACKS: toward directable thin shells". *ACM Transactions on Graphics* 26.3 (July 2007), 50. DOI: 10.1145/1276377.1276439 2.

[BW98] BARAFF, DAVID and WITKIN, ANDREW. "Large steps in cloth simulation". *ACM Conference on Computer Graphics and Interactive Techniques*. SIGGRAPH '98. 1998. DOI: 10.1145/280814.280821 1.

[BZKR17] BOG, TINO, ZANDER, NILS, KOLLMANNSBERGER, STEFAN, and RANK, ERNST. "Weak imposition of frictionless contact constraints on automatically recovered high-order, embedded interfaces using the finite cell method". *Computational Mechanics* 61.4 (Aug. 2017), 385–407. DOI: 10.1007/s00466-017-1464-6 3.

[CCK*21] CHEN, ZHEN, CHEN, HSIAO-YU, KAUFMAN, DANNY M., et al. "Fine Wrinkling on Coarsely Meshed Thin Shells". *ACM Transactions on Graphics* 40.5 (Aug. 2021), 1–32. DOI: 10.1145/3462758 2.

[CG91] CELNIKER, GEORGE and GOSSARD, DAVE. "Deformable curve and surface finite-elements for free-form shape design". *ACM SIGGRAPH Computer Graphics* 25.4 (July 1991), 257–266. DOI: 10.1145/127719.122746 3.

[CKSV23] CHEN, ZHEN, KAUFMAN, DANNY, SKOURAS, MÉLINA, and VOUGA, ETIENNE. "Complex Wrinkle Field Evolution". *ACM Transactions on Graphics* 42.4 (July 2023), 1–19. DOI: 10.1145/3592397 2.

[COS00] CIRAK, FEHMI, ORTIZ, MICHAEL, and SCHRÖDER, PETER. "Subdivision surfaces: a new paradigm for thin-shell finite-element analysis". *International Journal for Numerical Methods in Engineering* 47.12 (2000). DOI: 10.1002/(SICI)1097-0207(20000430)47:12<2039::AID-NME872>3.0.CO;2-1 3.

[CSvRV18] CHEN, HSIAO-YU, SASTRY, ARNAV, van REES, WIM M., and VOUGA, ETIENNE. "Physical simulation of environmentally induced thin shell deformation". *ACM Transactions on Graphics* 37.4 (July 2018), 1–13. DOI: 10.1145/3197517.3201395 2, 3, 5, 12.

[CTT17] CLYDE, DAVID, TERAN, JOSEPH, and TAMSTORF, RASMUS. "Modeling and data-driven parameter estimation for woven fabrics". *ACM SIGGRAPH/Eurographics Symposium on Computer Animation*. SCA '17. July 2017. DOI: 10.1145/3099564.3099577 2, 3.

[CXY*23] CHEN, YUNUO, XIE, TIANYI, YUKSEL, CEM, et al. "Multi-Layer Thick Shells". *ACM Conference on Computer Graphics and Interactive Techniques*. SIGGRAPH '23. July 2023. DOI: 10.1145/3588432.3591489 3.

[DKS13] DORNISCH, W., KLINKEL, S., and SIMEON, B. "Isogeometric Reissner–Mindlin shell analysis with exactly calculated director vectors". *Computer Methods in Applied Mechanics and Engineering* 253 (Jan. 2013), 491–504. DOI: 10.1016/j.cma.2012.09.010 3.

[DKWB18] DEUL, CRISPIN, KUGELSTADT, TASSILO, WEILER, MARCEL, and BENDER, JAN. "Direct Position-Based Solver for Stiff Rods". *Computer Graphics Forum*. 2018. DOI: 10.1111/cgf.13326 2.

[EOB13] ECHTER, R., OESTERLE, B., and BISCHOFF, M. "A hierarchic family of isogeometric shell finite elements". *Computer Methods in Applied Mechanics and Engineering* 254 (Feb. 2013), 170–180. DOI: 10.1016/j.cma.2012.10.018 3.

[ESK09] EFRATI, E., SHARON, E., and KUPFERMAN, R. "Elastic theory of unconstrained non-Euclidean plates". *Journal of the Mechanics and Physics of Solids* 57.4 (Apr. 2009), 762–775. DOI: 10.1016/j.jmps.2008.12.004 3.

[FB11] FRÖHLICH, STEFAN and BOTSCH, MARIO. "Example-Driven Deformations Based on Discrete Shells". *Computer Graphics Forum* 30.8 (Aug. 2011), 2246–2257. DOI: 10.1111/j.1467-8659.2011.01974.x 3.

[FJZ*23] FERGUSON, ZACHARY, JAIN, PRANAV, ZORIN, DENIS, et al. "High-Order Incremental Potential Contact for Elastodynamic Simulation on Curved Meshes". *ACM Conference on Computer Graphics and Interactive Techniques*. SIGGRAPH '23. July 2023. DOI: 10.1145/3588432.3591488 1, 3, 9.

[FLL*24] FERNÁNDEZ-FERNÁNDEZ, JOSÉ ANTONIO, LANGE, RALPH, LAIBLE, STEFAN, et al. "STARK: A Unified Framework for Strongly Coupled Simulation of Rigid and Deformable Bodies with Frictional Contact". *2024 IEEE International Conference on Robotics and Automation (ICRA)*. 2024 8.

[FLS*21] FERGUSON, ZACHARY, LI, MINCHEN, SCHNEIDER, TESEO, et al. "Intersection-Free Rigid Body Dynamics". *ACM Transactions on Graphics* 40.4 (July 2021). DOI: 10.1145/3450626.3459802 3.

[FLW*23] FERNÁNDEZ-FERNÁNDEZ, JOSÉ ANTONIO, LÖSCHNER, FABIAN, WESTHOFEN, LUKAS, et al. "SymX: Energy-based Simulation from Symbolic Expressions". (Feb. 2023). Preprint. DOI: 10.48550/ARXIV.2303.02156. arXiv: 2303.02156 [cs.CE] 7.

[FOZ95] FLORES, F. G., OÑATE, E., and ZARATE, F. "New assumed strain triangles for non linear shell analysis". *Computational Mechanics* 17.1–2 (Dec. 1995), 107–114. DOI: 10.1007/bf00356483 3.

[FP16] FORTUNATO, MEIRE and PERSSON, PER-OLOF. "High-order unstructured curved mesh generation using the Winslow equations". *Journal of Computational Physics* 307 (Feb. 2016), 1–14. DOI: 10.1016/j.jcp.2015.11.020 3.

[GGRZ06] GRINSPUN, EITAN, GINGOLD, YOTAM, REISMAN, JASON, and ZORIN, DENIS. "Computing discrete shape operators on general meshes". *Computer Graphics Forum* 25.3 (Sept. 2006), 547–556. DOI: 10.1111/j.1467-8659.2006.00974.x 2.

[GGWZ07] GARG, AKASH, GRINSPUN, EITAN, WARDETZKY, MAX, and ZORIN, DENIS. "Cubic Shells". *ACM SIGGRAPH/Eurographics Symposium on Computer Animation*. SCA '07. 2007. DOI: 10.2312/SCA/SCA07/091-098 2.

[GHDS03] GRINSPUN, EITAN, HIRANI, ANIL N., DESBRUN, MATHIEU, and SCHRÖDER, PETER. "Discrete Shells". SCA '03. 2003. DOI: 10.2312/SCA03/062-067 1–3.

[GHF*18] GUO, QI, HAN, XUCHEN, FU, CHUYUAN, et al. "A material point method for thin shells with frictional contact". *ACM Transactions on Graphics* 37.4 (July 2018), 1–15. DOI: 10.1145/3197517.3201346 3.

[GKS02] GRINSPUN, EITAN, KRYSL, PETR, and SCHRÖDER, PETER. "CHARMS: a simple framework for adaptive simulation". *ACM Transactions on Graphics* 21.3 (July 2002), 281–290. DOI: 10.1145/566654.566578 2, 3.

[GKT*24] GREEN, M.D., KIRILOV, K.S., TURNER, M., et al. "NekMesh: An open-source high-order mesh generation framework". *Computer Physics Communications* 298 (May 2024), 109089. DOI: 10.1016/j.cpc.2024.109089 3.

[GTS02] GREEN, SETH, TURKIYYAH, GEORGE, and STORTI, DUANE. "Subdivision-based multilevel methods for large scale engineering simulation of thin shells". *Proceedings of the seventh ACM symposium on Solid modeling and applications*. SM '02. June 2002. DOI: 10.1145/566282.566321 2.

[HLP96] HAKULA, H., LEINO, Y., and PITKÄRANTA, J. "Scale resolution, locking, and high-order finite element modelling of shells". *Computer Methods in Applied Mechanics and Engineering* 133.3–4 (July 1996), 157–182. DOI: 10.1016/0045-7825(95)00939-6 8.

[IW18] IMS, JEREMY and WANG, Z. J. "Automated low-order to high-order mesh conversion". *Engineering with Computers* 35.1 (Mar. 2018), 323–335. DOI: 10.1007/s00366-018-0602-x 3.

[KE22] KIM, THEODORE and EBERLE, DAVID. "Dynamic Deformables: Implementation and Production Practicalities (Now with Code!)": *ACM SIGGRAPH 2022 Courses*. SIGGRAPH '22. 2022. DOI: 10.1145/3532720.3535628. URL: https://www.tkim.graphics/DYNAMIC_DEFORMABLES/ 3.

[KGBG09] KAUFMANN, PETER, GISCHIG, SEBASTIAN MARTIN, BOTSCH, MARIO, and GROSS, MARKUS. *Implementation of discontinuous Galerkin Kirchhoff-Love shells*. Tech. rep. ETH Zürich, 2009. DOI: 10.3929/ETHZ-A-006733717 3.

[Kim20] KIM, THEODORE. "A Finite Element Formulation of Baraff-Witkin Cloth". *Computer Graphics Forum* 39.8 (Nov. 2020), 171–179. DOI: 10.1111/cgf.14111 1.

[KS16] KUGELSTADT, TASSILO and SCHÖMER, ELMAR. "Position and Orientation Based Cosserat Rods". *ACM SIGGRAPH/Eurographics Symposium on Computer Animation*. SCA '16. 2016, 1–10. DOI: 10.2312/SCA.20161234 2, 3.

[LB04] LEE, PHILL-SEUNG and BATHE, KLAUS-JÜRGEN. "Development of MITC isotropic triangular shell finite elements". *Computers & Structures* 82.11–12 (May 2004), 945–962. DOI: 10.1016/j.compstruc.2004.02.004 3.

[LBC12] LONG, QUAN, BURKHARD BORNEMANN, P., and CIRAK, FEHMI. "Shear-flexible subdivision shells". *International Journal for Numerical Methods in Engineering* 90.13 (Apr. 2012), 1549–1577. DOI: 10.1002/nme.3368 3.

[LDB*23] LE, QIQIN, DENG, YITONG, BU, JIAMU, et al. "Second-Order Finite Elements for Deformable Surfaces". *SIGGRAPH Asia 2023 Conference Papers*. SA '23. Dec. 2023. DOI: 10.1145/3610548.3618186 3, 8.

[LFJ*23] LÖSCHNER, FABIAN, FERNÁNDEZ-FERNÁNDEZ, JOSÉ ANTONIO, JESKE, STEFAN RHYS, et al. "Micropolar Elasticity in Physically-Based Animation". *Proceedings of the ACM on Computer Graphics and Interactive Techniques* 6.3 (Aug. 2023), 1–24. DOI: 10.1145/3606922 2–4, 6–8, 10, 11.

[LFS*20] LI, MINCHEN, FERGUSON, ZACHARY, SCHNEIDER, TESEO, et al. "Incremental potential contact: intersection-and inversion-free, large-deformation dynamics". *ACM Transactions on Graphics* 39.4 (Aug. 2020). DOI: 10.1145/3386569.3392425 3, 7, 9.

[LKJ21] LI, MINCHEN, KAUFMAN, DANNY M., and JIANG, CHENFANFU. "Codimensional incremental potential contact". *ACM Transactions on Graphics* 40.4 (July 2021), 1–24. DOI: 10.1145/3450626.3459767 3, 7, 8.

[LLB14] LEE, YOUNGYU, LEE, PHILL-SEUNG, and BATHE, KLAUS-JÜRGEN. "The MITC3+ shell element and its performance". *Computers & Structures* 138 (July 2014), 12–23. DOI: 10.1016/j.compstruc.2014.02.005 3.

[LLF*23] LONGVA, ANDREAS, LÖSCHNER, FABIAN, FERNÁNDEZ-FERNÁNDEZ, JOSÉ ANTONIO, et al. "Pitfalls of Projection: A study of Newton-type solvers for incremental potentials". (Nov. 2023). Preprint. DOI: 10.48550/ARXIV.2311.14526. arXiv: 2311.14526 [cs.GR] 8, 9.

[LLJ*20] LÖSCHNER, FABIAN, LONGVA, ANDREAS, JESKE, STEFAN, et al. "Higher-Order Time Integration for Deformable Solids". *ACM SIGGRAPH/Eurographics Symposium on Computer Animation*. SCA '20. 2020. DOI: 10.1111/cgf.14110 13.

[LLK*20] LONGVA, ANDREAS, LÖSCHNER, FABIAN, KUGELSTADT, TASSILO, et al. "Higher-order finite elements for embedded simulation". *ACM Transactions on Graphics* 39.6 (Nov. 2020), 1–14. DOI: 10.1145/3414685.3417853 3.

[LZRJ19] LI, YIPENG, ZHAO, XINGLIN, RAY, NAVAMITA, and JIAO, XIANGMIN. "Compact feature-aware Hermite-style high-order surface reconstruction". *Engineering with Computers* 37.1 (July 2019), 187–210. DOI: 10.1007/s00366-019-00815-z 3.

[MC10] MÜLLER, MATTHIAS and CHENTANEZ, NUTTAPONG. "Wrinkle Meshes". *ACM SIGGRAPH/Eurographics Symposium on Computer Animation*. SCA '10. 2010. DOI: 10.2312/SCA/SCA10/085-091 2.

[Mey00] MEYER, CARL D. *Matrix analysis and applied linear algebra*. First Edition. Society for Industrial and Applied Mathematics, 2000. 718 pp. ISBN: 9780898714548 4.

[MK23] MERCIER-AUBIN, ALEXANDRE and KRY, PAUL G. "Adaptive Rigidification of Discrete Shells". *Proceedings of the ACM on Computer Graphics and Interactive Techniques* 6.3 (Aug. 2023), 1–17. DOI: 10.1145/3606932 2.

[MLMG20] MAGISANO, DOMENICO, LEONETTI, LEONARDO, MADEO, ANTONIO, and GARCEA, GIOVANNI. "A large rotation finite element analysis of 3D beams by incremental rotation vector and exact strain measure with all the desirable features". *Computer Methods in Applied Mechanics and Engineering* 361 (Apr. 2020), 112811. DOI: 10.1016/j.cma.2019.112811 8.

[NBO15] NEFF, PATRIZIO, BÎRSAN, MIRCEA, and OSTERBRINK, FRANK. "Existence Theorem for Geometrically Nonlinear Cosserat Micropolar Model Under Uniform Convexity Requirements". *Journal of Elasticity* 121.1 (Feb. 2015), 119–141. DOI: 10.1007/s10659-015-9517-6 3, 10.

[Nef04] NEFF, PATRIZIO. "A geometrically exact Cosserat shell-model including size effects, avoiding degeneracy in the thin shell limit. Part I: Formal dimensional reduction for elastic plates and existence of minimizers for positive Cosserat couple modulus". *Continuum Mechanics and Thermodynamics* 16.6 (Oct. 2004), 577–628. DOI: 10.1007/s00161-004-0182-4 3, 5, 6.

[NPO13] NARAIN, RAHUL, PFAFF, TOBIAS, and O'BRIEN, JAMES F. "Folding and crumpling adaptive sheets". *ACM Transactions on Graphics* 32.4 (July 2013), 1–8. DOI: 10.1145/2461912.2462010 2.

[NR08] NOELS, L. and RADOVITZKY, R. "A new discontinuous Galerkin method for Kirchhoff–Love shells". *Computer Methods in Applied Mechanics and Engineering* 197.33–40 (June 2008), 2901–2929. DOI: 10.1016/j.cma.2008.01.018 3.

[NSBN23] NEBEL, LISA JULIA, SANDER, OLIVER, BÎRSAN, MIRCEA, and NEFF, PATRIZIO. "A geometrically nonlinear Cosserat shell model for orientable and non-orientable surfaces: Discretization with geometric finite elements". *Computer Methods in Applied Mechanics and Engineering* 416 (Nov. 2023), 116309. DOI: 10.1016/j.cma.2023.116309 2–6, 8, 10, 12.

[NSO12] NARAIN, RAHUL, SAMII, ARMIN, and O'BRIEN, JAMES F. "Adaptive anisotropic remeshing for cloth simulation". *ACM Transactions on Graphics* 31.6 (Nov. 2012), 1–10. DOI: 10.1145/2366145.2366171 2.

[Pai02] PAI, DINESH K. "Strands: Interactive simulation of thin solids using cosserat models". *Computer Graphics Forum*. Vol. 21. 3. 2002, 347–352. DOI: 10.1111/1467-8659.00594 2, 3.

[Qua12] QUAGLINO, ALESSIO. "Membrane locking in discrete shell theories". PhD thesis. Georg-August-Universität Göttingen, 2012. DOI: 10.53846/goediss-2533 8.

[RK13] RÉMILLARD, OLIVIER and KRY, PAUL G. "Embedded thin shells for wrinkle simulation". *ACM Transactions on Graphics* 32.4 (July 2013), 1–8. DOI: 10.1145/2461912.2462018 2.

[San12] SANDER, OLIVER. "Geodesic finite elements on simplicial grids". *International Journal for Numerical Methods in Engineering* 92.12 (June 2012), 999–1025. DOI: 10.1002/nme.4366 3.

[San15] SANDER, OLIVER. "Geodesic finite elements of higher order". *IMA Journal of Numerical Analysis* 36.1 (May 2015), 238–266. DOI: 10.1093/imanum/drv016 3.

[SB12] SIFAKIS, EFTYCHIOS and BARBIC, JERNEJ. "FEM Simulation of 3D Deformable Solids". *ACM SIGGRAPH 2012 Courses*. SIGGRAPH '12. Aug. 2012, 1–50. DOI: 10.1145/2343483.2343501. URL: http://www.femdefo.org/ 3.

[SB95] SANSOUR, CARLO and BEDNARCZYK, HERBERT. "The Cosserat surface as a shell model, theory and finite-element formulation". *Computer Methods in Applied Mechanics and Engineering* 120.1–2 (Jan. 1995), 1–32. DOI: 10.1016/0045-7825(94)00054-q 2, 3.

[SBS23] STEIGMANN, DAVID J., BÎRSAN, MIRCEA, and SHIRANI, MILAD. *Lecture Notes on the Theory of Plates and Shells: Classical and Modern Developments*. Springer Nature Switzerland, 2023. ISBN: 9783031256738. DOI: 10.1007/978-3-031-25674-5 5.

[SE10] SHARON, ERAN and EFRATI, EFI. "The mechanics of non-Euclidean plates". *Soft Matter* 6.22 (2010), 5693. DOI: 10.1039/c0sm00479k 3, 5.

[SF89] SIMO, J.C. and FOX, D.D. "On a stress resultant geometrically exact shell model. Part I: Formulation and optimal parametrization". *Computer Methods in Applied Mechanics and Engineering* 72.3 (Mar. 1989), 267–304. DOI: 10.1016/0045-7825(89)90002-9 2, 3.

[SFR90] SIMO, J.C., FOX, D.D., and RIFAI, M.S. "On a stress resultant geometrically exact shell model. Part III: Computational aspects of the nonlinear theory". *Computer Methods in Applied Mechanics and Engineering* 79.1 (Mar. 1990), 21–70. DOI: 10.1016/0045-7825(90)90094-3 2, 3.

[SGK19] SMITH, BREANNAN, GOES, FERNANDO DE, and KIM, THEODORE. "Analytic Eigensystems for Isotropic Distortion Energies". *ACM Transactions on Graphics* 38.1 (Feb. 2019), 1–15. DOI: 10.1145/3241041 13.

[SHD*18] SCHNEIDER, TESEO, HU, YIXIN, DUMAS, JÉRÉMIE, et al. "Decoupling simulation accuracy from mesh quality". *ACM Transactions on Graphics* 37.6 (Dec. 2018), 1–14. DOI: 10.1145/3272127.3275067 3.

[SHG*22] SCHNEIDER, TESEO, HU, YIXIN, GAO, XIFENG, et al. "A Large-Scale Comparison of Tetrahedral and Hexahedral Elements for Solving Elliptic PDEs with the Finite Element Method". *ACM Transactions on Graphics* 41.3 (Mar. 2022), 1–14. DOI: 10.1145/3508372 3.

[SHST12] STOMAKHIN, ALEXEY, HOWES, RUSSELL, SCHROEDER, CRAIG, and TERAN, JOSEPH M. "Energetically consistent invertible elasticity". *ACM SIGGRAPH/Eurographics Symposium on Computer Animation*. SCA '12. 2012, 25–32 13.

[SK23] SHI, ALVIN and KIM, THEODORE. "A Unified Analysis of Penalty-Based Collision Energies". *ACM SIGGRAPH/Eurographics Symposium on Computer Animation*. SCA '23. Aug. 2023, 1–19. DOI: 10.1145/3606934 13.

[SKH*21] SHAO, HAN, KUGELSTADT, TASSILO, HÄDRICH, TORSTEN, et al. "Accurately Solving Rod Dynamics with Graph Learning". *Advances in Neural Information Processing Systems*. Vol. 34. 2021 2.

[SNB16] SANDER, OLIVER, NEFF, PATRIZIO, and BÎRSAN, MIRCEA. "Numerical treatment of a geometrically nonlinear planar Cosserat shell model". *Computational Mechanics* 57.5 (Feb. 2016), 817–841. DOI: 10.1007/s00466-016-1263-5 2–4, 6, 8, 10.

[SPZ21] SCHNEIDER, TESEO, PANOZZO, DANIELE, and ZHOU, XIANLIAN. "Isogeometric high order mesh generation". *Computer Methods in Applied Mechanics and Engineering* 386 (Dec. 2021), 114104. DOI: 10.1016/j.cma.2021.114104 3.

[ST07] SPILLMANN, JONAS and TESCHNER, MATTHIAS. "CORDE: Cosserat Rod Elements for the Dynamic Simulation of One-Dimensional Elastic Objects". *ACM SIGGRAPH/Eurographics Symposium on Computer Animation*. SCA '07. 2007, 63–72. DOI: 10.2312/SCA/SCA07/063-072 2, 3.

[STC*12] SCHUMACHER, CHRISTIAN, THOMASZEWSKI, BERNHARD, COROS, STELIAN, et al. "Efficient Simulation of Example-Based Materials". *ACM SIGGRAPH/Eurographics Symposium on Computer Animation*. 2012. DOI: 10.2312/SCA/SCA12/001-008 3.

[TPM18] TURNER, MICHAEL, PEIRÓ, JOAQUIM, and MOXEY, DAVID. "Curvilinear mesh generation using a variational framework". *Computer-Aided Design* 103 (Oct. 2018), 73–91. DOI: 10.1016/j.cad.2017.10.004 3.

[TWS06] THOMASZEWSKI, BERNHARD, WACKER, MARKUS, and STRASSER, WOLFGANG. "A Consistent Bending Model for Cloth Simulation with Corotational Subdivision Finite Elements". *ACM SIGGRAPH/Eurographics Symposium on Computer Animation*. SCA '06. 2006. DOI: 10.2312/SCA/SCA06/107-116 2, 3.

[VSWH14] VETTER, ROMAN, STOOP, NORBERT, WITTEL, FALK K, and HERRMANN, HANS J. "Simulating Thin Sheets: Buckling, Wrinkling, Folding and Growth". *Journal of Physics: Conference Series* 487 (Mar. 2014), 012012. DOI: 10.1088/1742-6596/487/1/012012 3.

[WB23] WEN, JIAHAO and BARBIČ, JERNEJ. "Kirchhoff-Love Shells with Arbitrary Hyperelastic Materials". *ACM Transactions on Graphics* 42.6 (Dec. 2023), 1–15. DOI: 10.1145/3618405 1–3, 6, 7, 11.

[Wei12] WEISCHEDEL, CLARISSE. "A discrete geometric view on shear-deformable shell models". PhD thesis. Georg-August-Universität Göttingen, 2012. DOI: 10.53846/goediss-2453 2, 3, 8, 13.

[WHP11] WAWRZINEK, ANNA, HILDEBRANDT, KLAUS, and POLTHIER, KONRAD. "Koiter's Thin Shells on Catmull-Clark Limit Surfaces". *Vision, Modeling and Visualization*. VMV '11. 2011. DOI: 10.2312/PE/VMV/VMV11/113-120 3.

[WK23] WU, HAOMIAO and KIM, THEODORE. "An Eigenanalysis of Angle-Based Deformation Energies". *ACM SIGGRAPH/Eurographics Symposium on Computer Animation*. SCA '23. Aug. 2023, 1–19. DOI: 10.1145/3606929 13.

[WKS*11] WEBER, DANIEL, KALBE, THOMAS, STORK, ANDRÉ, et al. "Interactive deformable models with quadratic bases in Bernstein–Bézier-form". *The Visual Computer* 27.6–8 (Apr. 2011), 473–483. DOI: 10.1007/s00371-011-0579-6 3.

[WMA*15] WEBER, DANIEL, MUELLER-ROEMER, JOHANNES, ALTENHOFEN, CHRISTIAN, et al. "Deformation simulation using cubic finite elements and efficient p-multigrid methods". *Computers & Graphics* 53 (Dec. 2015), 185–195. DOI: 10.1016/j.cag.2015.06.010 3.

[WWB24] WEN, JIAHAO, WANG, BOHAN, and BARBIČ, JERNEJ. "Large-Strain Surface Modeling Using Plasticity". *IEEE Transactions on Visualization and Computer Graphics* (2024), 1–13. DOI: 10.1109/tvcg.2023.3289811 3.

[YZHY19] YANG, HONG Q., ZHOU, XIANLIAN, HARRIS, ROBERT E., and YANG, SIMON. "An Open Source, Geometry Kernel Based High-Order Element Mesh Generation Tool". *AIAA Scitech 2019 Forum*. Jan. 2019. DOI: 10.2514/6.2019-1719 3.

[ZDF*22] ZHANG, JIAYI ERIS, DUMAS, JÉRÉMIE, FEI, YUN (RAYMOND), et al. "Progressive Simulation for Cloth Quasistatics". *ACM Transactions on Graphics* 41.6 (Nov. 2022), 1–16. DOI: 10.1145/3550454.3555510 2.

[ZDF*23] ZHANG, JIAYI ERIS, DUMAS, JÉRÉMIE, FEI, YUN (RAYMOND), et al. "Progressive Shell Qasistatics for Unstructured Meshes". *ACM Transactions on Graphics* 42.6 (Dec. 2023), 1–17. DOI: 10.1145/3618388 2.